

Technical Paper

Suffusion in densely compacted Satozuka pumice sand and its impact on static loading undrained shear strength and dilation behaviour

Rupali Sarmah ^{a,*}, Yoichi Watabe ^b

^a Soil Mechanics Laboratory, Graduate School of Engineering, Hokkaido University, Kita 13, Nishi 8, Sapporo 060-8628, Japan

^b Soil Mechanics Laboratory, Faculty of Engineering, Hokkaido University, Kita 13, Nishi 8, Sapporo 060-8628, Japan

Received 27 May 2023; received in revised form 11 October 2023; accepted 24 October 2023

Available online 23 November 2023

Abstract

Pumice sand of volcanic origin contains a high fraction of non-plastic fines (>40 % for Satozuka pumice sand in Sapporo, Japan). Suffusion in such soil can wash away a portion of the fine particles and alter the soil microstructure. The moisture content and degree of compaction can affect the suffusion characteristics of soil deposits, however their effect has not yet been evaluated. Future construction sites in growing Sapporo City, consisting of pumice sand, will require a high degree of compaction (over 90 % and preferably over 95 %) as this sand is prone to suffusion in spite of its dense state. The aim of this study is to assess the impact of suffusion on densely compacted pumice sand with a high proportion of fines, based on its mechanical properties, with an emphasis on shear strength and dilatancy. Firstly, the suffusion characteristics of Satozuka pumice sand were evaluated. Subsequently, undrained triaxial tests (\overline{CU} tests) under monotonic loading were conducted on high-density specimens, with suffusion and without suffusion, to study the impact of suffusion. It is seen in the results that the hydraulic conductivity, shear strength, stress paths, and dilatancy are all noticeably affected by suffusion. The specimens with suffusion exhibit an increase in residual shear strength and maximum deviator stress under shearing and experience an earlier occurrence of phase transformation from contraction to dilation during shearing. This tendency implies that suffusion has no significant negative impact on the deterioration of earth fill made from pumice sand and non-plastic fines, and that it persists at degrees of compaction between 80 % and 100 %.

© 2023 Production and hosting by Elsevier B.V. on behalf of The Japanese Geotechnical Society. This is an open access article under the CC BY-NC-ND license (<http://creativecommons.org/licenses/by-nc-nd/4.0/>).

Keywords: Pumice sand; Suffusion; Hydraulic conductivity; Shear strength; Dilatancy

1. Introduction

The area of Satozuka in Sapporo City, Japan stands on a layer of pumice sand of volcanic origin (or pyroclastic flow deposit) derived approximately 40,000 years ago from Mount Shikotsu (currently a caldera of Lake Shikotsu). In order to accommodate the growing demand for residential land, the southern and eastern suburbs of Sapporo have been developed in recent decades by excavating the hills made of pumice sand and filling in the valleys (Fig. 1). Part

of this artificially developed residential area in Satozuka liquefied and suffered significant ground subsidence as a consequence of the Hokkaido Eastern Iburi Earthquake (2018).

Satozuka pumice sand typically contains more than 40 % non-plastic fine particles. Cubrinovski et al. (2010) stated that the liquefaction resistance of sandy soil decreases with an increase in the non-plastic fine content up to 30 %. The liquefaction that happened in the Satozuka area concurs with this previous research, even though the fine content is larger than 30 %. In spite of this, the geotechnical investigation conducted immediately after the earthquake revealed the occurrence of suffusion inside

* Corresponding author.

E-mail address: rupali_sarmah5@eis.hokudai.ac.jp (R. Sarmah).

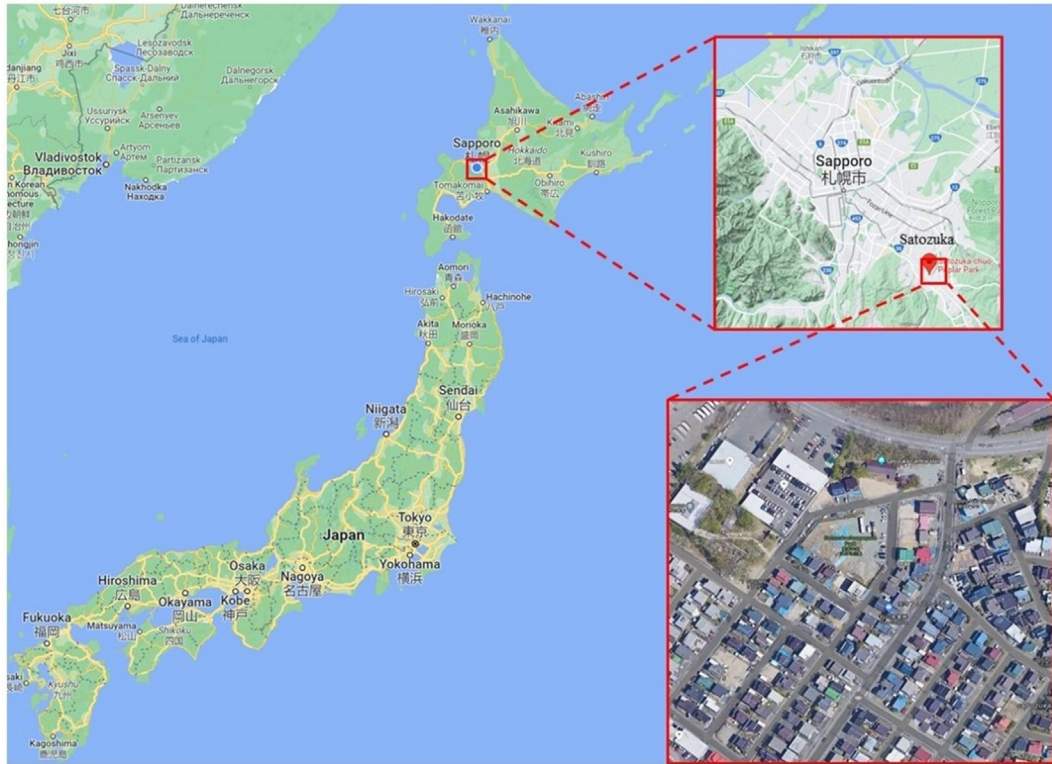


Fig. 1. Location and aerial view of artificially developed residential area of Satozuka, Japan. (Source: <https://www.google.co.jp/maps>).

the network of underground drainage pipes installed beneath the artificially developed area (Fig. 2), causing a reduction in fines. Several layers of muddy cakes were found inside the drain pipes and at the drain culvert intersections, suggesting that suffusion may have taken place prior to the earthquake.

Suffusion is a type of internal erosion; it is the process of the migration of fine soil particles through coarse soil particles under the action of a hydraulic gradient (Fig. 3). This phenomenon can alter the microstructure of natural and

artificial soil deposits, thus changing the geo-mechanical behaviour of soils under different stress states (Chang and Zhang, 2011; Xiao and Shiwihat, 2012). Soil liquefaction resistance can be evaluated by its dilation tendency under monotonic and cyclic loading triaxial tests (Elgamal et al., 1998; Sladen et al., 1985). It is crucial, therefore, to explore how suffusion affects the dilation behaviour of pumice sand deposits before attempting to interpret the liquefaction mechanism of suffusion-induced pumice sand.



Fig. 2. (a) Evidence of suffusion (Watabe and Nishimura, 2020), and (b) layers of muddy cake inside underground drainage pipes installed beneath artificially developed area.

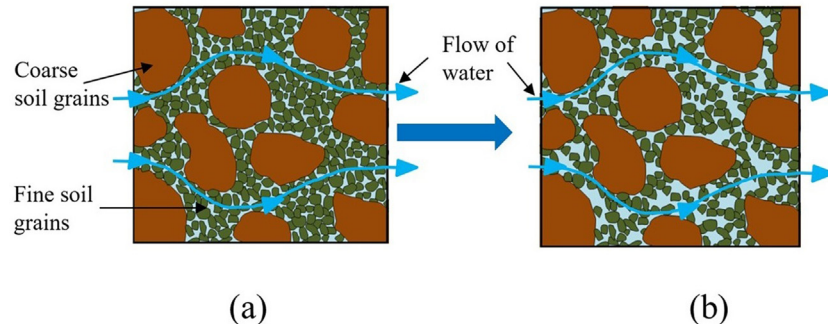


Fig. 3. Illustration of suffusion phenomenon (a) before suffusion, and (b) after suffusion.

[Ke and Takahashi \(2014\)](#) investigated the undrained and drained monotonic loading behaviour of gap-graded non-cohesive eroded soil and concluded that the peak deviator stress of the eroded specimen was relatively higher than that of the specimen without erosion. [Sato and Kuwano \(2018\)](#) studied the effect of a small degree of suffusion due to downward seepage flow on the stiffness and deformation of well-graded natural sand containing plastic clay particles. They reported that an increase in void ratio and the reconstitution of the soil packing after suffusion resulted in a decrease in soil stiffness. [Chitravel et al. \(2021\)](#) evaluated the effect of internal erosion on the monotonic response and stiffness degradation of reconstituted non-plastic volcanic ash (pumice sand) by conducting undrained and drained triaxial tests on eroded specimens prepared in loose packing with relative densities of 30 %, 50 %, and 80 % and with moisture content higher than the optimum value ($w = 47\%$). They observed that internal erosion has a positive influence on brittleness and the peak strength of loose soil, and found that the elastic yield surface of eroded soil specimens expanded. [Bedja et al. \(2022\)](#) investigated the influence of suffusion on the mechanical behaviour of gap-graded granular soil with non-plastic fines under drained and undrained conditions, and reported that eroded specimens were less contractive and showed a decrease in undrained strength. These previous studies imply that the mechanical behaviour of suffusion-induced soil is very complex and differs depending on many factors, such as soil type, gradation, packing, test conditions, etc.

[Tatsuoka et al. \(2016\)](#) recommended that artificially compacted soil should achieve a degree of compaction over 90 %, preferably over 95 %, for the design and construction of earth fill. As Sapporo is the central hub in the northern part of Japan and is still growing, future construction sites in expanded areas of the city will require a high degree of compaction. The prior study on the internal erosion of volcanic ash by [Chitravel et al. \(2021\)](#) was performed in loose packing which is similar to the in-situ conditions in the liquefied region of Satozuka as it subsists at present (artificially compacted approximately 40 years ago). The influence of suffusion on the mechanical behaviour of densely packed volcanic soil, meeting the above-mentioned construction management practice (degree of compaction over 90 % or 95 %), still remains a key issue. The aim of this study is to investigate whether densely compacted pumice

sand, containing a high fraction of fines, is secured against suffusion or not on the basis of undrained shear strength, as the effect of suffusion on the mechanical properties of pumice sand under this type of compaction condition has not been previously studied. Furthermore, [Watabe et al. \(2021\)](#) experimented on the erodibility of clayey sand (with a grain size distribution similar to that of pumice sand with plastic fines) and stated that the degree of saturation (a function of the moisture content and compaction condition) affects the erodibility of soil. The influence of the variation in the degree of saturation on suffusion has scarcely been examined for well-graded volcanic soil with a high non-plastic fines content, denoting a deficiency in the understanding of the role of the soil microfabric in suffusion.

This paper describes the results of a laboratory study of the mechanical behaviour of suffusion-induced Satozuka pumice sand, particularly focusing on high-density specimens with a variation in moisture content. Firstly, the suffusion characteristics of Satozuka pumice sand were evaluated in respect to the influence of the moisture content ($w = 30\% \text{ to } 52\%$) and degree of compaction ($D_c = 80\% \text{ to } 100\%$) at a hydraulic gradient of 200. Subsequently, consolidated undrained triaxial tests ($\overline{\text{CU}}$ tests) under monotonic loading were conducted on specimens, with suffusion and without suffusion, to compare the impact of suffusion on the hydraulic conductivity, shear strength, stress path, and dilatancy properties. Next, the degree of compaction of the suffusion-induced soil is correlated with the maximum deviator stress, brittleness, critical state, and dilatancy. Then, the results are compared to those of specimens without suffusion. Finally, the resulting observations are interpreted to infer the changes in the soil microstructure.

2. Testing material

2.1. Soil properties

Pumice sand of volcanic origin, particular to the Satozuka region of Sapporo, Japan, was used in this study. The physical properties of this soil, obtained from the initial site investigation immediately after the Hokkaido Eastern Iburi Earthquake by [Watabe and Nishimura \(2020\)](#),

are included in **Table 1** (representing Series A). An optical microscopic photo and scanning electron microscopic (SEM) image revealed the presence of glassy plate-like sand particles with high angularity and the aggregation of fine particles (**Fig. 4**).

Another batch of soil was collected from Satozuka-Chuo Poplar Park a year later and the physical properties (representing Series B) were determined. The properties were different from those of Series A most likely because of the heterogeneity of the soil material and the non-uniformity of the compacted ground. The physical properties of both the Series A and Series B samples are summarized in **Table 1**. The collected pumice sand was dark greyish brown in color (**Fig. 5**) with a shiny smooth texture. Soil particles passing through a 9.5-mm mesh with the Series B physical properties were used for the preparation of the specimens in this study. The grain size distribution (**Fig. 6**) of the pumice sand indicates that the soil is well graded with an approximately 45 % non-plastic fines content (<0.075 mm). The optimum moisture content (*OMC*) and maximum dry density (ρ_{dmax}) were determined as 42.7 % and 1.068 Mg/m³, respectively, from standard Proctor compaction tests (**JIS A 1210**). The maximum and minimum densities of the soil were obtained as 0.988 Mg/m³ and 0.680 Mg/m³, respectively, from minimum and maximum density tests (**JIS A 1224**).

2.2. CT image analysis

X-ray CT (computer tomography) scans of the soil were conducted to grasp the variation in the microstructure of the soil with the degree of compaction. **Fig. 7** shows the reconstructed cross-sectional white background CT images of the soil specimens at 75 % and 100 % degrees of compaction (D_c) at the *OMC*. The gray scale in these CT images is white to black, corresponding to low to high density, which is the opposite of normal CT images. The aggregation of fine particles is observed in the specimens. The loose specimen shows the formation of a macropore network (macro-porosity) due to the aggregation of fine particles.

3. Experimental program

3.1. Testing equipment

The experimental setup is modelled after the suffusion apparatus by **Sato and Kuwano (2018)** and **Kuwano**

Table 1
Physical properties of Satozuka pumice sand.

Physical property	Series A	Series B
Soil particle density, ρ_s	2.391 Mg/m ³	2.395 Mg/m ³
Coefficient of uniformity, C_u	24	97
Coefficient of curvature, C_c	2.17	2.95
Maximum density, ρ_{max}	1.051 Mg/m ³	0.988 Mg/m ³
Minimum density, ρ_{min}	0.749 Mg/m ³	0.680 Mg/m ³
Optimum moisture content, <i>OMC</i>	42.6 %	42.7 %
Maximum dry density, ρ_{dmax}	1.094 Mg/m ³	1.068 Mg/m ³

et al. (2020) with several distinct instruments. It comprises a triaxial testing apparatus with a strain-controlled bottom loading frame, pressurized water supply system (erosion tank), and effluent collection container (**Fig. 8**). The triaxial testing apparatus consists of a loading frame, triaxial acrylic cell, submergible load cell, and two gauge-type pressure transducers. The volume change of the specimen can be measured with the help of a low-capacity differential pressure transducer (LCDPT) connected to a volume gauge. The vertical displacement of the specimen was measured in terms of motor displacement, and the radial strain was calculated from the volume change and vertical displacement. A visual basic (VB) computer program was used to operate the apparatus as well as to obtain and record the test results.

To facilitate the migration of fines, the main bodies of the pedestal and cap were tapered into a funnel shape leading to a hole in the center, and thus, making provision for suffusion. A porous plate was attached to the modified body with screws. To allow the finer particles to erode, filters made of metal mesh and plastic mesh (1-mm openings for both) were placed above the porous plate (**Fig. 9**).

3.2. Test procedure

The experimental program consisted of five test stages, namely, specimen preparation, saturation, consolidation, suffusion by hydraulic gradient, and shearing. Soil specimens, 100 mm in height and 50 mm in diameter, were prepared by compacting the soil in layers at approximately 80 %, 90 %, 95 %, and 100 % degrees of compaction (D_c) on dry and wet sides of the *OMC* of the compaction curve. The target compaction conditions of the test specimens are shown in **Fig. 10**. According to **Tamura and Sakai (1992)**, the degree of compaction is defined as the ratio of the soil density measured at the in-situ condition (ρ_d) to the maximum dry density of the soil (ρ_{dmax}) obtained from the standard Proctor compaction test. Mathematically, D_c at a specific moisture content can be expressed as

$$D_c = \frac{\rho_d}{\rho_{dmax}} \quad (1)$$

where ρ_d is the dry density of a specimen at that moisture content and ρ_{dmax} is the maximum dry density of the soil at the *OMC*. The test specimen identities, as well as the target and attained compaction conditions, are presented in **Table 2**.

The specimens were saturated by the double vacuum method followed by the infiltration of water at a backpressure of 300 kPa. They were considered to be saturated when the value of Skempton's pore pressure parameter (*B*-value) exceeded 0.95 (**Skempton, 1954**). After achieving the desired *B*-value, the specimens were consolidated to an effective stress of 80 kPa.

The consolidated specimens were subjected to suffusion by application of a hydraulic gradient. At the beginning of the suffusion stage, the pressure at the top of the specimen

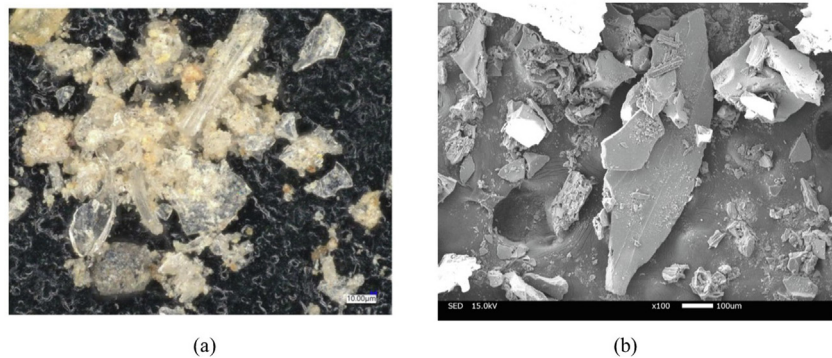


Fig. 4. (a) Optical microscopic photo, and (b) scanning electron microscopic (SEM) image of Satozuka pumice sand (Watabe and Nishimura, 2020).



Fig. 5. Satozuka pumice sand.

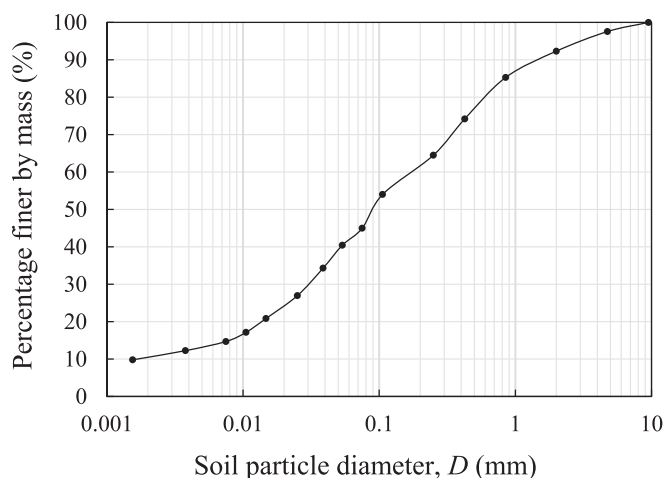


Fig. 6. Grain size distribution curve of Satozuka pumice sand.

was kept at 50 kPa, while the atmospheric pressure (0 kPa) at the bottom of the specimen was maintained by connecting the bottom part to the effluent collection bowl. The cell pressure/total radial pressure surrounding the specimen was maintained at 130 kPa, resulting in an effective stress of 80 kPa at the top of the specimen during this stage. The backpressure at the top cap was increased stepwise 50 kPa every 30 min, and the water carrying the eroded soil was col-

lected. The backpressure was increased to induce the desired hydraulic gradient. The total radial pressure was simultaneously increased to ensure that the 80 kPa effective stress was maintained at the top of the specimen. Stepwise increases in the cell pressure/total radial pressure and the water pressure/backpressure at the top cap were continued until the pressure difference between the top cap and the bottom pedestal reached 200 kPa, thus creating a maximum hydraulic gradient of 200. Fig. 10(b) shows the changes in pressure inside (backpressure) and outside (cell pressure/total radial pressure) the specimen with time. After the completion of the suffusion tests, the backpressure on the specimen was increased to 300 kPa before the shearing stage to maintain identical test conditions for all specimens (both WS-series and WoS-series) during shearing.

While a hydraulic gradient of 200 may seem too large, it can still be achieved under practical conditions, such as the presence of a small crack or opening on the surface of a drainage pipe leading to leakage. For such conditions, the equipotential lines will be concentrated around the leakage point where the pore pressure distribution becomes equivalent to the hydrostatic pressure in the fill ground, and the water will be directed to flow through a thin layer wrapping around the drainage pipe located at the bottom of the compacted earth fill, as shown in Fig. 11. Under such conditions, this phenomenon may lead to a high hydraulic gradient of up to 200, although it is highly unlikely to exceed this value.

The effluent containing eroded fines was collected in a water tank (during saturation) or an effluent collection bowl (during suffusion tests) and each volume was thereafter stirred separately to make a suspension. The quantity of eroded fines present in the effluent was measured in terms of turbidity using a portable digital nephelometric turbidimeter and converted to a concentration of soil in a soil + water sample (in terms of dry mass, g/L). Afterwards, the amount of fines, in terms of the dry mass, was calculated by multiplying the concentration by the effluent volume.

Afterwards, undrained triaxial compression tests (CU tests) were conducted at the strain rate of 0.1 %/min and terminated when the axial strain (ϵ_a) reached 15 %, keeping a cell pressure of 380 kPa and a backpressure of 300 kPa. A

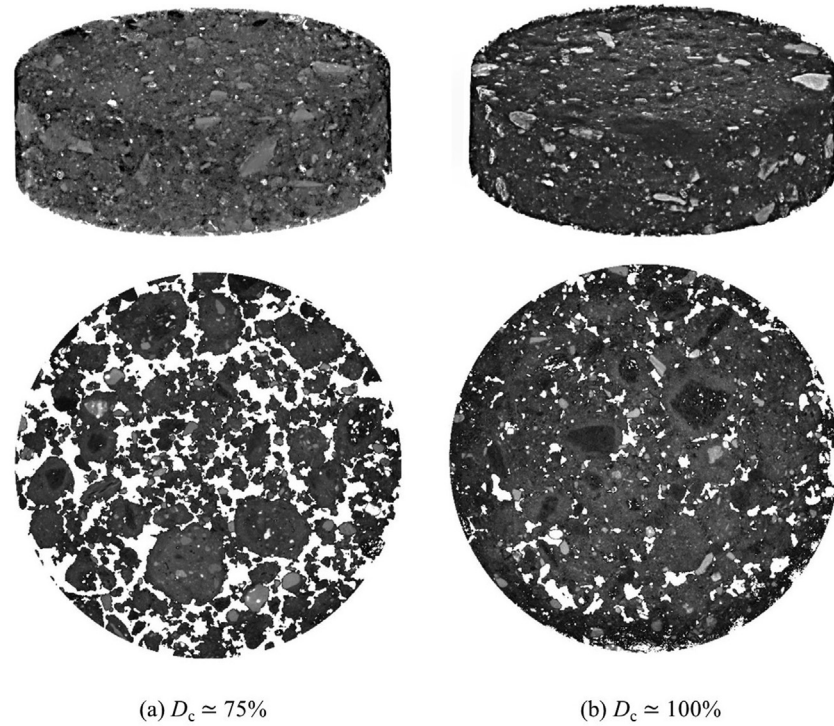


Fig. 7. CT images of pumice sand.

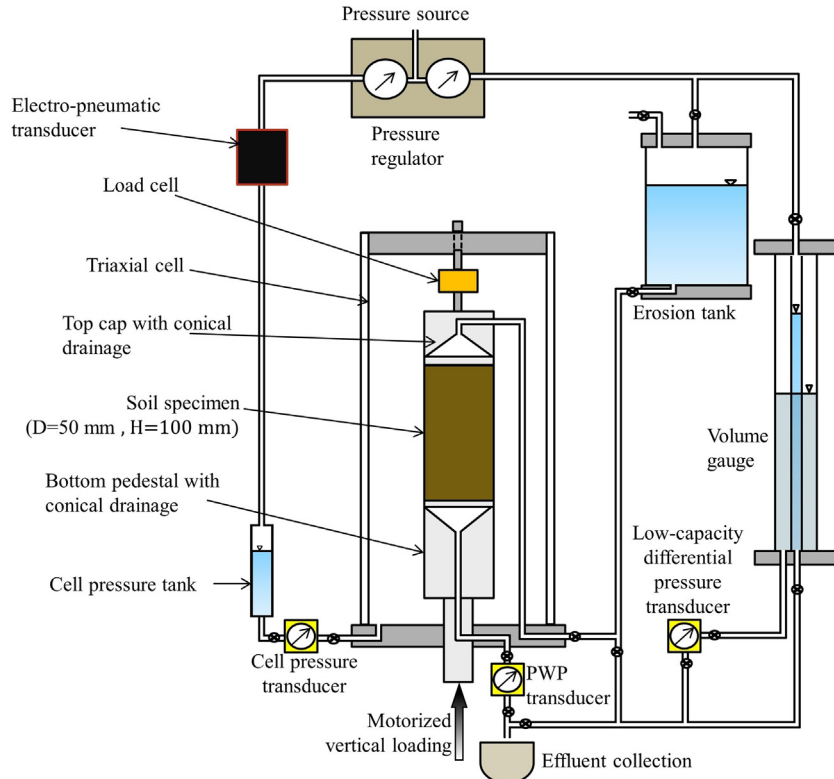


Fig. 8. Schematic of experimental setup.

detailed account of the procedures at different test stages can be found in Sarmah et al. (2021). CU tests on the specimens without suffusion, prepared in a similar method and

subjected to 380 kPa of cell pressure and 300 kPa of back-pressure, were also conducted to compare the effect of suffusion on the WS-series specimens.

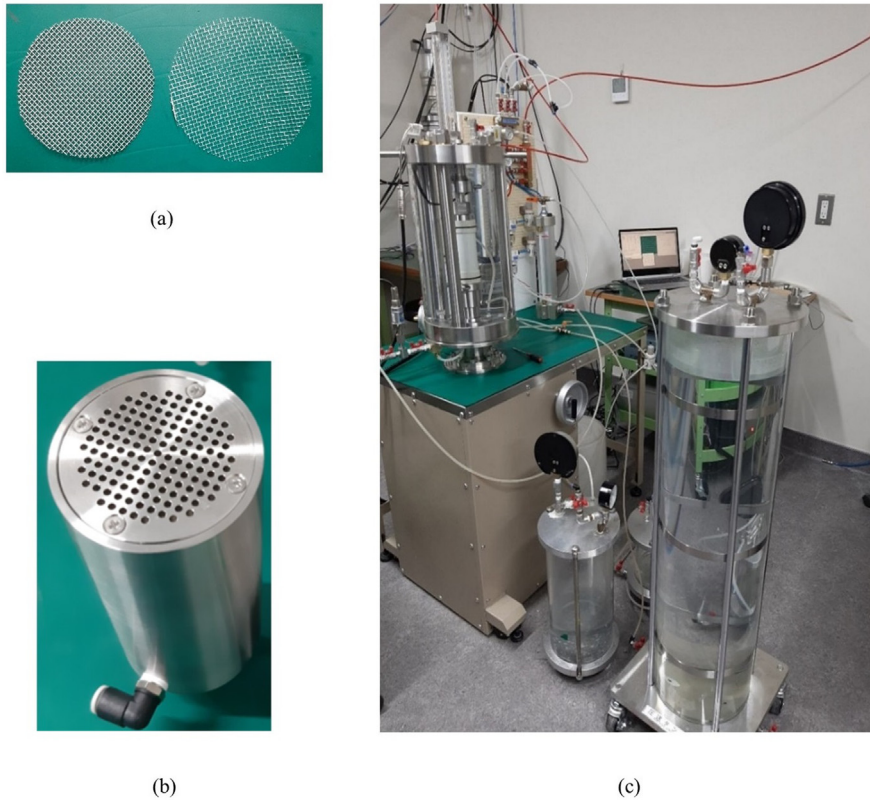


Fig. 9. Assembly of experimental setup (a) metal mesh (left) and plastic mesh (right) to control size of eroded particles, (b) modified pedestal with attached porous plate, and (c) complete triaxial setup with erosion tank.

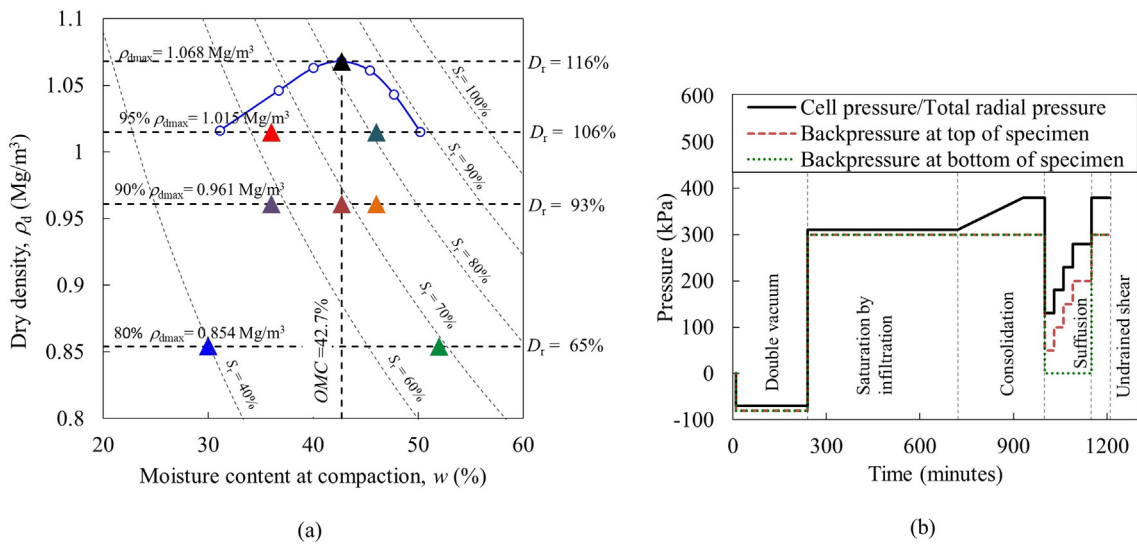


Fig. 10. (a) Compaction curve with target compaction conditions of specimens, and (b) changes in pressure inside and outside specimens with time during different stages.

4. Test results and discussion

4.1. Effect of compaction condition on degree of suffusion

The results of the suffusion tests are shown in Table 3 in terms of the dry mass of the eroded fines. The specimens

eroded during saturation even though the difference in pressure between the top and bottom of the specimen was, at most, 20 kPa. The amount of fines that eroded during saturation was measured for the collected effluent using a turbidimeter. The results show that the specimens lost a substantial number particles due to migration during this

Table 2

Test specimen identities with target and attained degrees of compaction as well as moisture content during specimen preparation.

Specimen identity (Test case)	Target degree of compaction, $D_{c,t}$ (%)	Attained degree of compaction, D_c (%)	Moisture content, w (%)	Degree of saturation, S_r (%)	Suffusion occurred
WS_80Dc_30w	80	81.53	29.9	41	Yes
WoS_80Dc_30w	80	81.87	29.9	41	No
WS_80Dc_52w	80	81.67	52.4	72	Yes
WoS_80Dc_52w	80	81.69	50.8	70	No
WS_90Dc_36w	90	90.94	35.8	59	Yes
WoS_90Dc_36w	90	90.30	36.4	59	No
WS_90Dc_omc	90	91.46	43.2	71	Yes
WoS_90Dc_omc	90	91.38	42.9	71	No
WS_90Dc_46w	90	90.41	45.9	74	Yes
WoS_90Dc_46w	90	91.32	45.2	73	No
WS_95Dc_36w	95	94.65	36.0	63	Yes
WoS_95Dc_36w	95	94.20	36.7	63	No
WS_95Dc_46w	95	95.84	46.4	83	Yes
WoS_95Dc_46w	95	96.04	45.9	82	No
WS_100Dc_omc	100	99.71	42.5	82	Yes
WoS1_100Dc_omc	100	99.82	42.4	81	No
WoS2_100Dc_omc	100	100.78	41.5	81	No

* WS and WoS stand for “with suffusion” and “without suffusion” conditions, respectively.

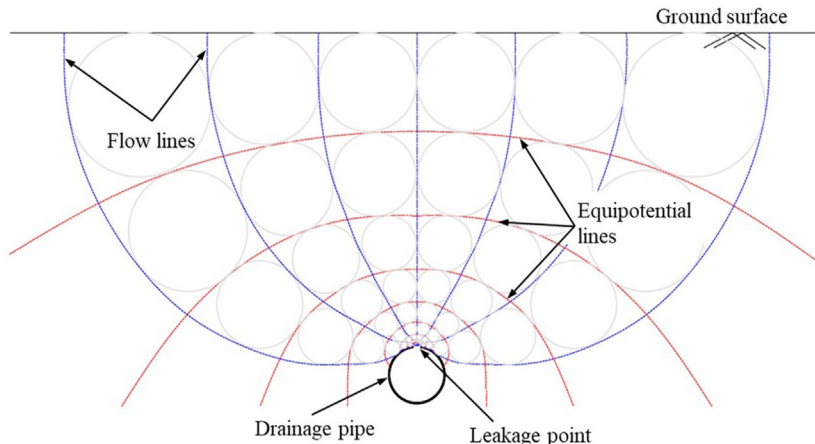


Fig. 11. Flow network for leakage point on drainage pipe.

Table 3

Results of suffusion tests under various compaction conditions and moisture contents.

Specimen identity	Dry mass of soil eroded during saturation, (g)	Dry mass of soil eroded during suffusion by hydraulic gradient, (g)	Total dry mass of soil eroded, (g)	Percentage of total fines eroded, (%)	Hydraulic conductivity at $i = 50$, k_{i50} (10^{-6} m/s)	Hydraulic conductivity at $i = 200$, k_{i200} (10^{-6} m/s)
WS_80Dc_30w	5.97	2.99	8.96	5.27	7.34	3.28
WS_80Dc_52w	3.68	2.23	5.92	3.58	2.98	1.87
WS_90Dc_36w	3.41	0.98	4.39	2.29	2.91	1.74
WS_90Dc_omc	1.02	1.16	2.18	1.16	3.35	1.86
WS_90Dc_46w	0.95	1.33	2.28	1.21	2.55	1.49
WS_95Dc_36w	1.07	1.07	2.14	1.08	14.6	4.35
WS_95Dc_46w	0.26	0.43	0.69	0.35	3.39	1.63
WS_100Dc_omc	0.07	1.35	1.42	0.68	0.95	0.85

stage, as shown in Fig. 12. During the suffusion tests (by the application of the hydraulic gradient), the eroded fines were sparse. However, the results are found to be consis-

tent with the erosion occurring during the actual suffusion tests, namely, within a similar range (0.22 % to 1.76 %), which indicates the reliability of the tests. The small

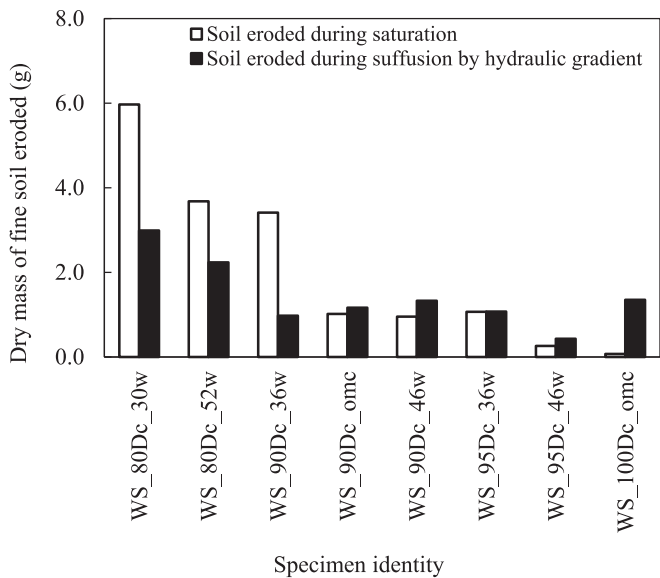


Fig. 12. Fractional distribution of particles that migrated in terms of dry mass in grams.

amount of erosion during the suffusion tests can be attributed to high density, high angularity, the small size of the specimens, and the fact that the majority of suffusion occurred involuntarily during the saturation stage, particularly the migration of the finer particles, which was unavoidable (Ke and Takahashi, 2014; Marot et al., 2012; Zhong et al., 2018). However, the total amount of soil that eroded during the saturation and suffusion processes can be regarded as the particles that eroded due to suffusion. Moreover, after the completion of each test, a considerable mass of fine particles was observed to have accumulated on the pedestal and porous plate surface. In an attempt to prevent the trapping of fines on the pedestal, the cone angle of the pedestal was increased at a later stage and tests were performed on the specimens with $D_c \approx 80\%$. Although the trapping of fines was minimized, it could not be eliminated completely. The fine particles trapped on the pedestal and porous plate were collected carefully in a beaker after the completion of the experiment and the oven-dried mass was obtained. Thereafter, the amount of soil that eroded during suffusion by the hydraulic gradient is expressed as the combination of the dry mass of the soil that eroded during the suffusion tests (obtained from the effluent collected using the turbidimeter) and the oven-dried mass of the soil that was trapped on the pedestal. Finally, in this research, the degree or extent of suffusion is expressed as the percentage of total dry mass of soil eroded (=total dry mass of soil eroded/dry mass of specimen during preparation) during the complete experiment (i.e., summation of the two elements shown in Fig. 12).

The relationship between degree of saturation S_r at compaction with the percentage of fines that eroded during saturation and the percentage of total fines that eroded are plotted in Fig. 13. If the suffusion tests (by the application of the hydraulic gradient) had been conducted directly

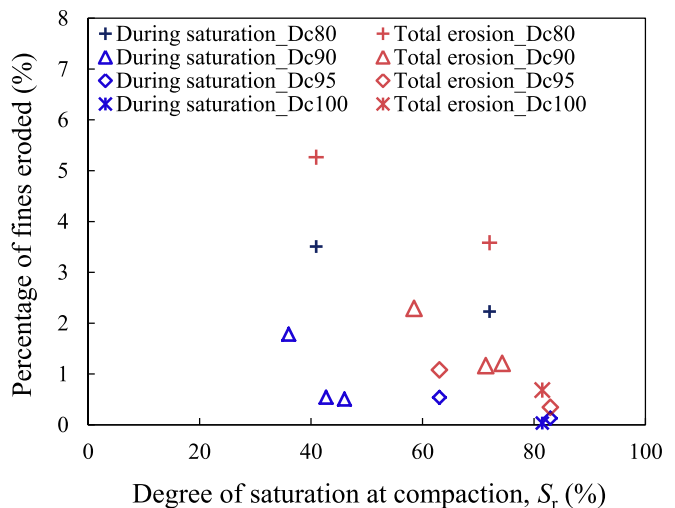


Fig. 13. Percentage of fines that eroded during saturation and suffusion corresponding to degree of saturation at compaction.

without the saturation or consolidation of the specimen, this would also have led to a high extent of erosion. Therefore, these two phenomena cannot be separated, and the total amount of erosion is seen as an important parameter to be considered when analyzing suffusion characteristics. For the case of $D_c \approx 80\%$ (i.e., relatively loose specimens), a comparatively high percentage of total fines is eroded from the specimens on both dry and wet sides of the compaction curve. Loose specimens possess a larger constriction size and decreased inter-particle grain to grain contact. This causes the easy detachment of the fines leading to the initiation of suffusion at a lower hydraulic gradient, thereby leaving a lesser amount to erode during actual suffusion. Moreover, the presence of higher effective confining stress leads to a lesser extent of erosion during suffusion (80 kPa) than the extent of erosion occurring during the saturation process (10 kPa) (Ke and Takahashi, 2014). For these reasons, the amount of erosion during saturation becomes larger than that during suffusion (by application of the hydraulic gradient) in loose specimens. In addition, it is observed that S_r adversely influences the extent of suffusion as lower saturation results in more erosion for equally compact specimens. This increase in the amount of migrated fines can be ascribed to the change in the soil microfabric due to the variation in S_r . The spatial arrangement of the soil particles and voids (patterns of soil constituents), studied in thin sections with the help of an optical microscope, scanning electron microscope, computer tomography, etc., is referred to as the soil microfabric (Miedema and Oort, 1990). Differences in the S_r and D_c of the soil alter the pore geometry, resulting in a change in the soil microfabric. Soil with low S_r at compaction (i.e., on the dry side of the OMC) develops a visible inter-pore network in the soil microfabric, called macro-porosity, while soil with high S_r at compaction (i.e., on the wet side of the OMC) develops invisible intra-pores in the fine particles, called micro-porosity. Macro-porosity allows more

water to pass through the soil, increasing the kinetic potential of the soil grains and influencing the detachment of fines from the soil matrix. For this reason, the presence of macro-porosity makes a soil more erodible. For the specimen with $D_c \approx 100\%$ at the OMC, it was found that the erosion occurring during saturation is trivial and that the majority of the fines migrated during suffusion by the application of the hydraulic gradient. This is due to the fact that the dense packing of soil creates a smaller constriction size, allowing a lesser amount of fines to detach and migrate under the low hydraulic gradient that developed during saturation.

4.2. Spatial deformation due to suffusion

The deformation of the specimens subjected to suffusion was found to be non-destructive and was not feasible to detect by simple visual observation. The spatial deformation of specimen WS_90Dc_omc, during suffusion by the hydraulic gradient, was determined using the stereophotogrammetry technique developed by Nishimura (2022). Fig. 14(a) presents the axial strain, while Fig. 14(b) presents the radial strain at the end of suffusion in the reconstructed image of the 3-dimensional space with compression as positive strain. At the end of suffusion, a maximum axial strain of 3% is spotted in a few elements in the lower part of the specimen, whereas axial deformation of less than 1% is detected in the upper and middle parts of the specimen. These observations indicate that the bottom surface of the specimen is more affected by suffusion than the other parts of the specimen. The radial strain is less than 1% on the left half (in the vertical plane) of the specimen, while the right half (in the vertical plane) shows nearly zero radial

strain. A maximum radial strain of 1.4% is observed near the top surface of the specimen. The marginal axial deformation and radial deformation on the top and middle parts of the specimen suggest that the erosion began in the upper part of the specimen, then the fines migrated to the lower part and clogged the pores, thus affecting the extent of suffusion in the lower part of the specimen (with the bottom surface as the exception). The face averages of the axial strain (ε_a) and radial strain (ε_r) are estimated as 0.110% and 0.295%, respectively, from the strain of each element obtained from the stereophotogrammetry analysis. Details on the determination of spatial deformation using a stereophotogrammetry analysis are provided in Appendix II.

4.3. Effect of suffusion on hydraulic conductivity

Hydraulic conductivity k of the WS-series specimens is determined from the volume of the effluent collected during the suffusion tests using Darcy's law which states

$$Q = \frac{V_e}{t} = kiA \quad (2)$$

where Q is the flow rate, V_e is the volume of effluent, t is the flow duration, i is the hydraulic gradient, and A is the area of the specimen. The hydraulic conductivity at the start of suffusion ($i = 50$) and that at the end of suffusion ($i = 200$) are listed in Table 3. The complex network of pores has made the flow path of the WS-series specimens twisted, causing tortuosity. Moreover, the flow path has become narrower due to clogging by the migrated fines which have been trapped at a bottleneck of the flow path. The flow path is further elongated by the random move-

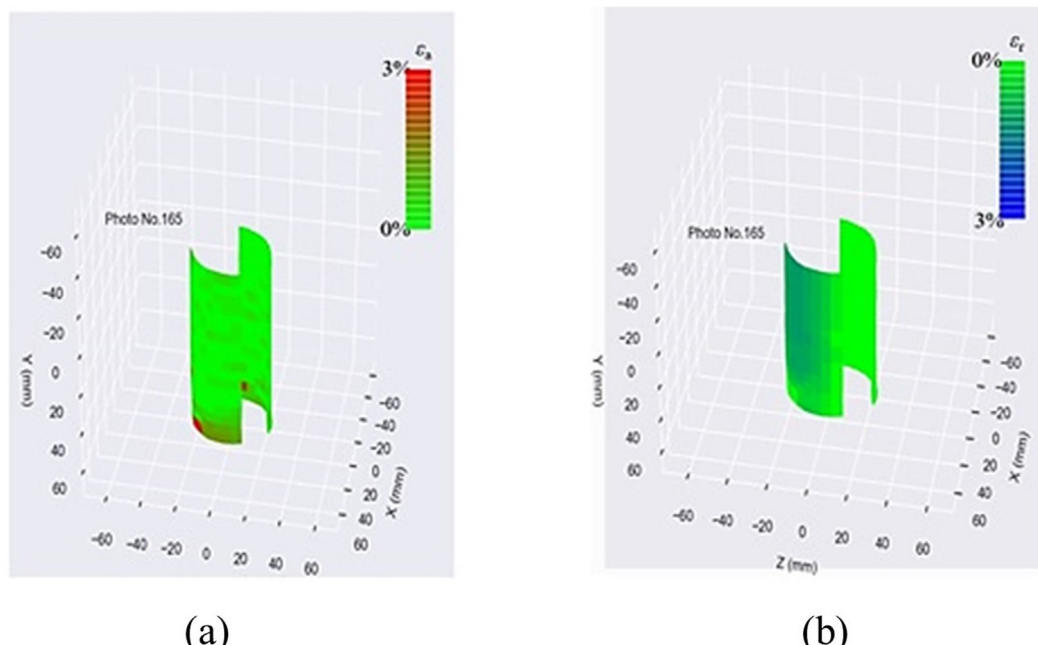
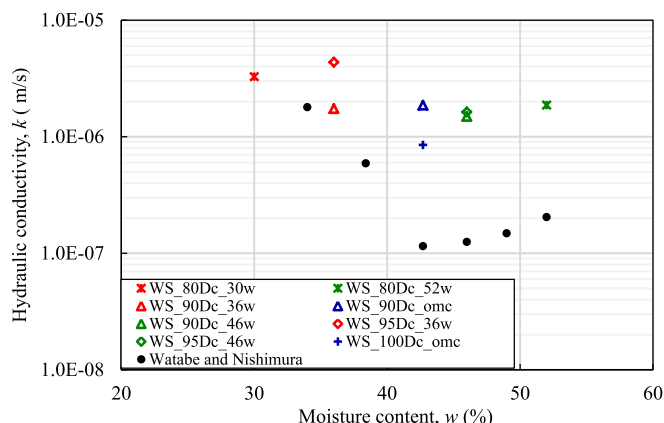


Fig. 14. Deformation observed in 3-dimensional reconstructed images at end of suffusion (a) axial strain, and (b) radial strain.

ment of fast-moving water through the narrow, bottlenecked pore network which has resulted in a decrease in k with an increase in i . A similar range in k after suffusion ($i = 200$), within the range of 8.5×10^{-7} to 4.5×10^{-6} m/s, is observed for all densities. [Watabe and Nishimura \(2020\)](#) determined the k of the specimens without suffusion at very high densities, i.e., D_c ranging from 96 % to 101 % along Proctor's normal compaction curve, as shown in [Fig. 15](#). The hydraulic conductivities of the very high-density WS-series specimens (WS_95Dc_36w, WS_95Dc_46w, and WS_100Dc_omc) at $i = 200$ have been significantly affected by suffusion compared to those in [Watabe and Nishimura \(2020\)](#), causing the k of the WS-series specimens to increase significantly. In summary, the removal of fine particles during the saturation process causes a significant increase in k , while the trapped fine particles clogged the flow path during the application of the hydraulic gradient, resulting in a slight decrease in final k . However, the absolute value of k before shear remains higher for the WS-series specimens which indicates an increase in voids, i.e., porosity, due to the removal of the fines.

4.4. Effect of suffusion on shear strength under various compaction conditions

The relationship between deviator stress q and axial strain ε_a under different degrees of compaction and moisture contents for both WS- and WoS-series specimens is depicted in [Fig. 16](#). The WoS-series specimens on the dry side of the OMC show strain-softening behaviour, whereas the WS-series specimens with similar compaction conditions display a similar tendency with the improvement in residual shear strength q_R . The WS-series specimens on both the wet side of the OMC and at the OMC exhibit stain-hardening behaviour with a significant increase in q_R for the WS-series specimens, although the D_c values of WS_90Dc_46w and WS_95Dc_46w are marginally smaller than those of WoS_90Dc_46w and WoS_95Dc_46w. Moreover, the value of q_R for the WS_100Dc_omc specimen ($D_c = 99.71$ %) is found to be 7 % lower than the



[Fig. 15. Hydraulic conductivity corresponding to moisture content.](#)

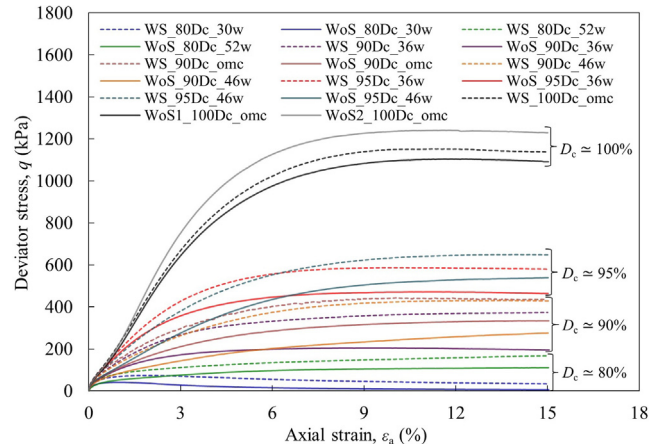


[Fig. 16. Relationship between deviator stress and axial strain.](#)

WoS-series specimen with $D_c = 100.78$ %. An additional experiment with another WoS-series specimen at $D_c = 99.82$ % was conducted to confirm this observation, and its q_R was found to have increased by 4 % compared to the WS-series specimen. These two test results apparently do not coincide with each other; however, this can be explained by taking into account the very high undrained residual shear strength of such densely packed specimens and their sensitivity to a minute variation in D_c . Therefore, at the very high degree of compaction of $D_c \approx 100$ %, the influence of suffusion on the residual shear strength is complex, yet not detrimental to pumice sand owing to its high strength.

The relationship between the brittleness index and the degree of compaction is shown in [Fig. 17\(a\)](#). Brittleness index I_B is an indicator of the soil's collapsibility during undrained triaxial shear and is defined as

$$I_B = \frac{q_{\max} - q_R}{q_{\max}} \quad (3)$$

where q_{\max} is the maximum deviator stress and q_R is the residual shear strength of the specimens ([Bishop, 1967](#); [Yoshimine et al., 1999](#)). The value of $I_B = 1$ indicates the complete loss of strength, while $I_B = 0$ signifies dilative behaviour and the absence of strain softening. The WoS_80Dc_30w specimen shows collapsible or brittle behaviour with a high I_B value which was reduced in the WS_80Dc_30w specimen, indicating lowered collapsibility ([Fig. 17\(b\)](#)). I_B values of nearly zero are observed in the case of the remaining specimens with no or only trivial changes in I_B for the WS-series specimens compared to the WoS-series specimens.

[Fig. 18](#) depicts a comparative study on the effect of suffusion on the maximum (or peak) deviator stress, q_{\max} , corresponding to density and moisture content conditions, as well as the existing research on suffusion for different types of soil. Suffusion tends to increase the q_{\max} for D_c up to 95 %. Specimens on the wet side of the OMC exhibit higher q_{\max} values than those on the dry side of the OMC with similar D_c for both WS and WoS-series specimens. [Sato](#)

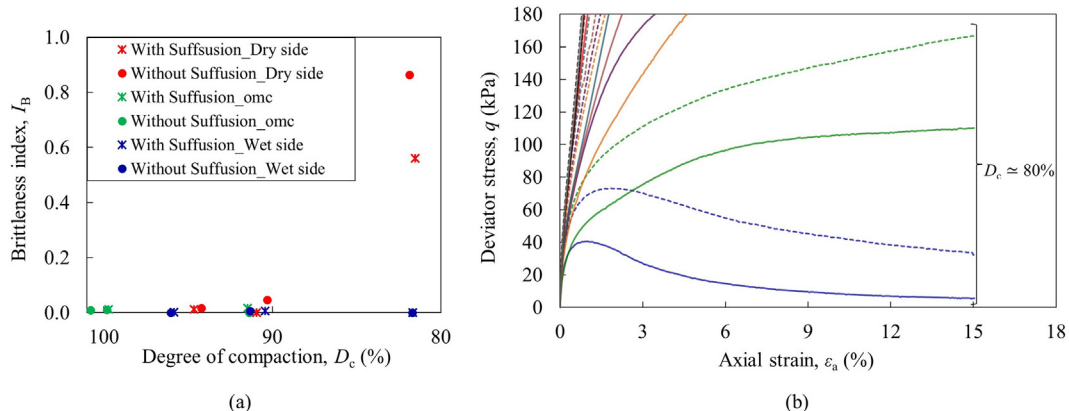


Fig. 17. Relationships between (a) brittleness index and degree of compaction, and (b) deviator stress and axial strain in enlarged scale to depict brittle behaviour of $D_c \approx 80\%$ specimens.

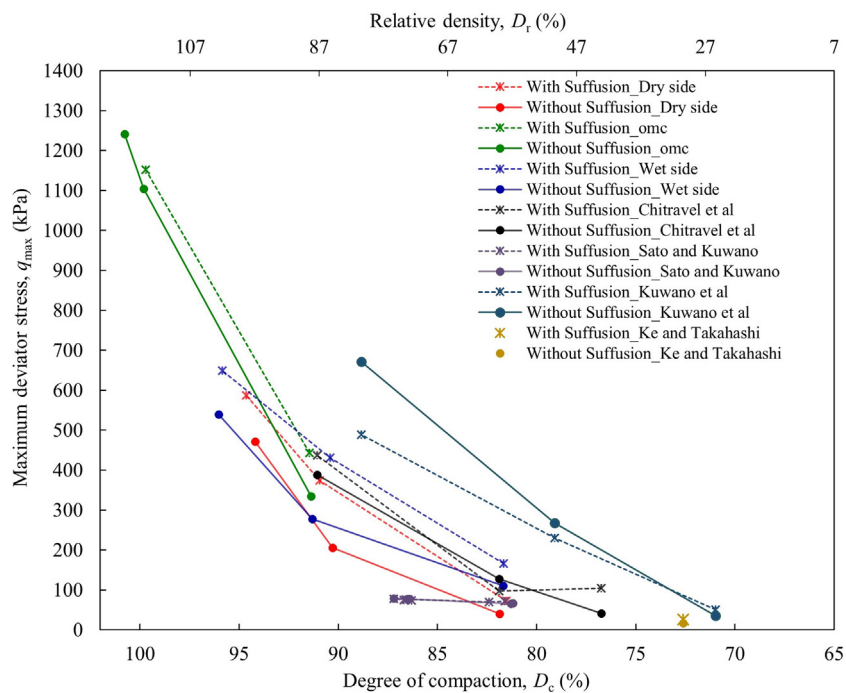


Fig. 18. Relationship between maximum deviator stress and degree of compaction.

and Kuwano (2018) and Ke and Takahashi (2014) reported an increase in the q_{max} of suffusion-induced cohesionless soil, whereas Kuwano et al. (2021) reported a decrease in the q_{max} of a cohesive soil mixture (silica and DL clay). Chitravel et al. (2021) conducted undrained shear tests on suffusion-induced reconstituted volcanic ash using the physical properties of Series A in Table 1. For comparison, Fig. 18 displays the values obtained by them in terms of D_c recalculated using the physical properties of Series B shown in Table 1. This is because the soils examined by Chitravel et al. (2021) were of both Series A and Series B provided by the authors' research group.

The normalized maximum deviator stress (q_{max}/σ'_c , where σ'_c is the effective consolidation stress), correspond-

ing to the degree of compaction with the moisture content condition, is shown in Fig. 19. Both the WS- and WoS-series specimens demonstrate an exponential increase in q_{max}/σ'_c with increasing D_c (i.e., density). The regression coefficients (coefficients of determination, R^2) for the exponential equations of the trend lines, without distinguishing between the dry and wet side specimens, are within an acceptable range (≥ 0.9) with values of 0.925 and 0.937 for the WS and WoS conditions, respectively.

4.5. Stress paths

Fig. 20 presents the effective stress paths (ESPs) of the WS- and WoS-series specimens. The ESP of the

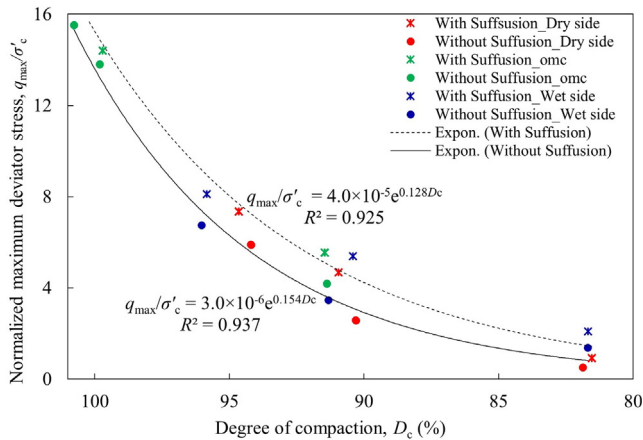


Fig. 19. Relationship between normalized maximum deviator stress and degree of compaction.

WoS_80Dc_30w specimen exhibits unstable behaviour by moving to the left and displays undrained instability resembling the static liquefaction tendency, which is improved in the WS_80Dc_30w specimen [Fig. 20(b)]. Static liquefaction is characterized by zero or negligible undrained shear strength due to the development of large excess pore water pressure (Yamamoto and Lade, 1997; Picarelli et al., 2020). The specimens on the wet side of the OMC at $D_c \approx 80\%$ exhibit unstable behaviour at the initial stage, which becomes stable later on, under both WS and WoS conditions. The rest of the specimens display stable behaviour for all the WS- and WoS-series specimens. Moreover, the $D_c \approx 80\%$ specimens (dry and wet sides) converge at the critical state line (CSL) whereas, for the rest of the specimens with $D_c \geq 90\%$, the ESPs do not appear to converge at the CSL as the slopes of the ESPs continue to decrease until the end of the experiment. This makes the determination of the slope of the CSL complex. Therefore, the slope of the ESP at q_{\max} , $M_{q\max}$, and the maximum slope of the ESP, M_{\max} , which are analogous to the slope of the CSL, are used in the following sections.

Fig. 21(a) displays the relationship among the degree of compaction, slope of the ESP at q_{\max} , $M_{q\max} = \frac{q_{\max}}{p'}$, and shear resistance angle at q_{\max} , $\phi_{q\max}$, for the WS- and WoS-series specimens. The value of $M_{q\max}$ increases in response to an increase in density with values ranging from 0.96 to 1.70. A higher $M_{q\max}$ is observed for the WS-series specimens for $D_c \approx 80\%$ (wet and dry sides), 90% (OMC), and 95% (dry side) compared to the $M_{q\max}$ of the similarly compacted WoS-series specimens. However, suffusion is not shown to generate any significant change in $M_{q\max}$ for $D_c \approx 100\%$ for the OMC specimens and reduces the $M_{q\max}$ marginally for the $D_c \approx 90\%$ (dry and wet sides) and $D_c \approx 95\%$ (wet side) specimens. The shear resistance angle at q_{\max} , $\phi_{q\max}$, corresponding to $M_{q\max}$, is calculated from the following relationship:

$$M_{q\max} = \frac{q_{\max}}{p'} = \frac{6 \sin \phi_{q\max}}{3 - \sin \phi_{q\max}} \quad (4)$$

in which a tendency similar to $M_{q\max}$, with values ranging from 24° to 42° , is displayed.

The maximum slopes of the ESPs, $M_{\max} = \left(\frac{q}{p'}\right)_{\max}$, are found to be in the range of 1.46 to 2.11, as shown in Fig. 21(b). For the dry side specimens, suffusion decreases M_{\max} for $D_c \approx 80\%$, but increases it for $D_c \approx 90\%$ and 95%. For specimens at the OMC, suffusion does not influence the M_{\max} significantly for $D_c \approx 90\%$ and decreases it for $D_c \approx 100\%$. For the wet side specimens, suffusion increases M_{\max} for $D_c \approx 80\%$ and 90%, and decreases it for $D_c \approx 95\%$. Maximum shear resistance angle ϕ_{\max} is calculated from the following relationship:

$$M_{\max} = \left(\frac{q}{p'}\right)_{\max} = \frac{6 \sin \phi_{\max}}{3 - \sin \phi_{\max}} \quad (5)$$

The values for ϕ_{\max} are all in the range of 24° to 42° and display a tendency similar to that of M_{\max} . The values for $\phi_{q\max}$ and ϕ_{\max} , shown in secondary scale in Fig. 21 (a) and (b), are calculated from the values for $M_{q\max}$ and M_{\max} in the respective primary scale using Eqs. (4) and (5). Therefore, the converted values for $\phi_{q\max}$ and ϕ_{\max} in secondary scale are not linear.

4.6. Dilation tendency and phase transformation points

The relationship between excess pore water pressure Δu and axial strain ϵ_a of the WS- and WoS-series specimens is shown in Fig. 22. The value of Δu continues to increase until it reaches a certain value and then remains constant (thereafter) in the $D_c \approx 80\%$ specimens on the dry side of the OMC. This signifies that the specimens tend to contract during undrained shear until reaching the peak Δu value, after which no change in total volume occurs although the axial strain increases. The rest of the specimens with $D_c \approx 80\%$ on the wet side of the OMC, as well as the $D_c \approx 90\%$, 95%, and 100% specimens on both the dry and wet sides of the OMC, show a decrease in Δu after reaching the peak value under both WS and WoS conditions. This peak signifies a change in the contractive behaviour from contraction to dilation which is called the phase transformation point (PTP) (Daouadji et al., 2016). The respective PTPs of every specimen are marked with downward arrows in Fig. 22. (b), (c), (d), and (e). Dilation is more significant in the high-density specimens under both WS and WoS conditions. The WS-series specimens exhibit a higher dilation tendency when compared to the WoS-series specimens. The WS-series specimens have lower Δu at the PTPs than the WoS-series specimens under a similar compaction condition (Table 4). The change in excess PWP and the normalized change in excess PWP are estimated as

$$\text{Change in excess PWP} = \Delta u_{\text{PTP}} - \Delta u_{15\%} \quad (6)$$

$$\text{Normalized change in excess PWP} = \frac{\Delta u_{\text{PTP}} - \Delta u_{15\%}}{\sigma'_c} \quad (7)$$

where Δu_{PTP} is the excess PWP at the PTP and $\Delta u_{15\%}$ is the excess PWP at an axial strain of 15%. Eq. (7) corresponds

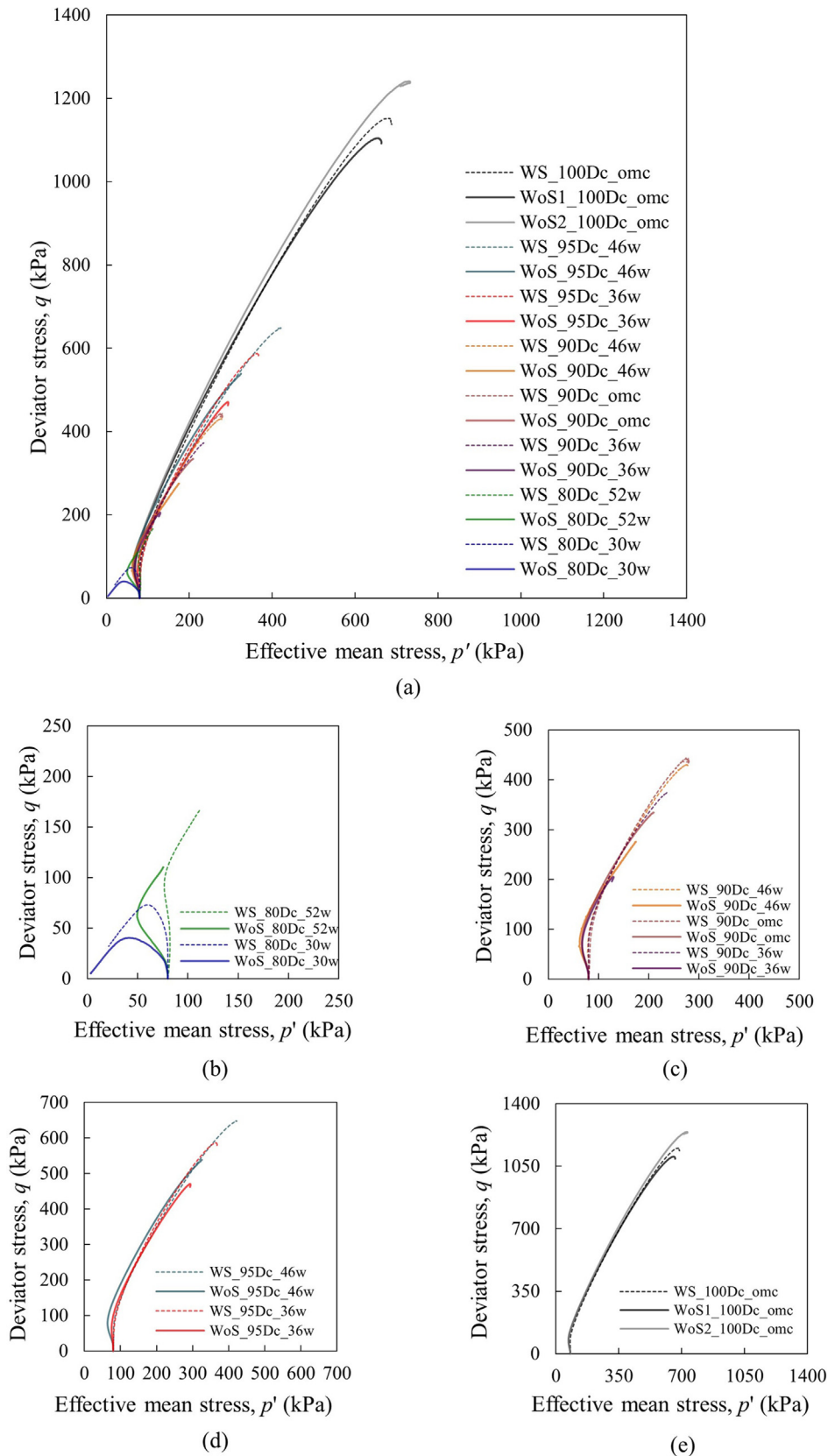


Fig. 20. Effective stress paths of (a) all specimens, (b) $D_c \approx 80\%$, (c) $D_c \approx 90\%$, (d) $D_c \approx 95\%$, and (e) $D_c \approx 100\%$.

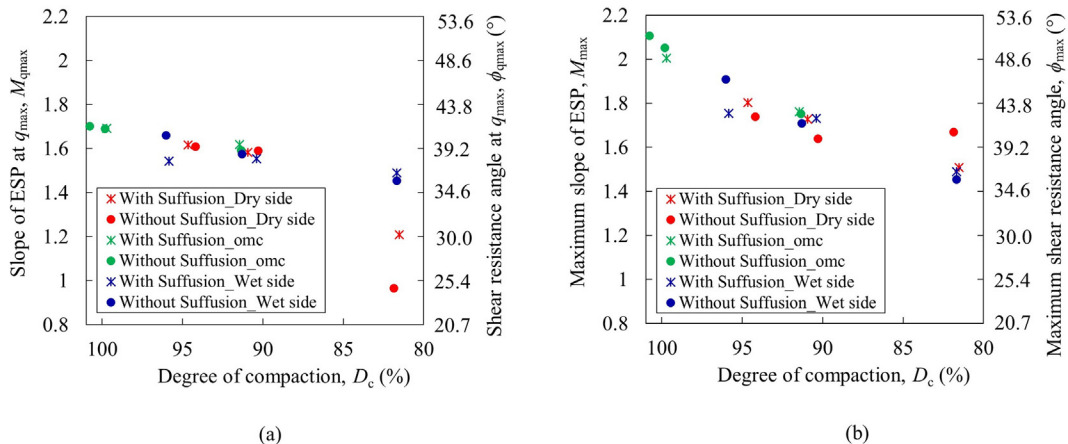


Fig. 21. Relationships among (a) slope of ESP at q_{\max} , shear resistance angle at q_{\max} , and degree of compaction, and (b) maximum slope of ESP, maximum shear resistance angle, and degree of compaction.

to the absolute value of the change in negative Δu generated due to dilation after the PTP. The initiation of suffusion primarily involves the migration of the finest particles, thereby resulting in a reduction in the particle size ratio and a shift of the soil towards homogeneity by the removal of fine grains at the end of suffusion. The particle size ratio is defined as the ratio of the diameter of the largest grains in a sample to the diameter of the smallest grains in the sample (Wiącek and Stasiak, 2018). As the particle size ratio decreases, there is a corresponding increase in the void ratio of the soil matrix. This results in a change in the soil matrix, resulting in an increase in the excess angle (the difference between the shearing resistance angle at q_{\max} , $\phi_{q\max}$, and the maximum shear resistance angle, ϕ_{\max} , of sand under the application of stress, finally increasing the dilatancy (Bolton, 1986; Xiao et al., 2014).

The relationship between the axial strain at the PTP, $\varepsilon_{a,PTP}$, and degree of compaction D_c is shown in Fig. 23. The increase in density is accompanied by a decrease in $\varepsilon_{a,PTP}$. The WS-series specimens reach the PTP at a lower axial strain, i.e., prior to that of the WoS-series specimens, indicating a lesser amount of contraction during shear. However, it is notable that the $\varepsilon_{a,PTP}$ of the WS-series specimens is lower than that of the WoS-series specimens at $D_c \simeq 95\%$ (dry side), and it is almost the same as that for both the WS- and WoS-series specimens with $D_c \simeq 100\%$ at the OMC.

The relationship between the normalized change in excess PWP and the D_c of the WS- and WoS-series specimens is shown in Fig. 24. In the density-dependent changes in Δu or dilation tendency, polynomial increases in the normalized change in excess PWP $[(\Delta u_{PTP} - \Delta u_{15\%})/\sigma'_c]$ are spotted with increasing density under both WS and WoS conditions. The regression coefficients (coefficients of determination, R^2) for the polynomial equations of the trend lines, without distinguishing between the dry and wet side specimens, are 0.975 and 0.983 for the WS and WoS conditions, respectively.

5. Microstructural changes in pumice sand due to suffusion

The geomechanical behaviour of natural and compacted soil depends on the arrangement of the solid soil components and soil pores, referred to as the soil microstructure (Romero et al., 1999; Tang et al., 2020). Changes in the mechanical behaviour of the WS-series specimens, compared to the WoS-series specimens, indicate an alteration in the soil microstructure.

Fig. 25(a) shows the variation in dry density ρ_d after the four stages of the experiment, namely, specimen preparation (stage 1), saturation (stage 2), consolidation (stage 3), and suffusion by hydraulic gradient/before shear (stage 4). The dry density after any stage n ($=1, 2, 3$, and 4) can be calculated using Eq. (8) as follows:

$$\rho_{d,n} = \frac{m_{d,n}}{V_n} = \frac{m_{d,n-1} - \Delta m_{d,n}}{V_{n-1} - \Delta V_n} \quad (8)$$

where $\rho_{d,n}$, $m_{d,n}$, and V_n are the dry density, mass of the dry soil, and volume of the soil specimen at stage n , respectively. In addition, $\Delta m_{d,n}$ and ΔV_n are the changes in the dry mass of the soil and volumetric deformation, respectively, of the soil specimen during stage n .

The loss of a major fraction of fines during saturation leads to a decrease in ρ_d of the WS-series specimens after saturation, except for the specimens with $D_c \simeq 95\%$ and 100%. A subsequent rise in ρ_d is observed in all specimens after consolidation. As seen in Fig. 13, the specimens on the dry side erode more than the specimens on the wet side at similar densities. This results in a drop in ρ_d during the saturation stage in the WS-series specimens on the dry side and a minor increase in ρ_d in the specimens on the wet side, except for the $D_c \simeq 80\%$ specimens. Finally, all the WS-series specimens have a lower or equivalent final ρ_d right before shearing than the WoS-series specimens. It is evident, therefore, that densification did not occur after suffusion and that it does not play a role in the change in

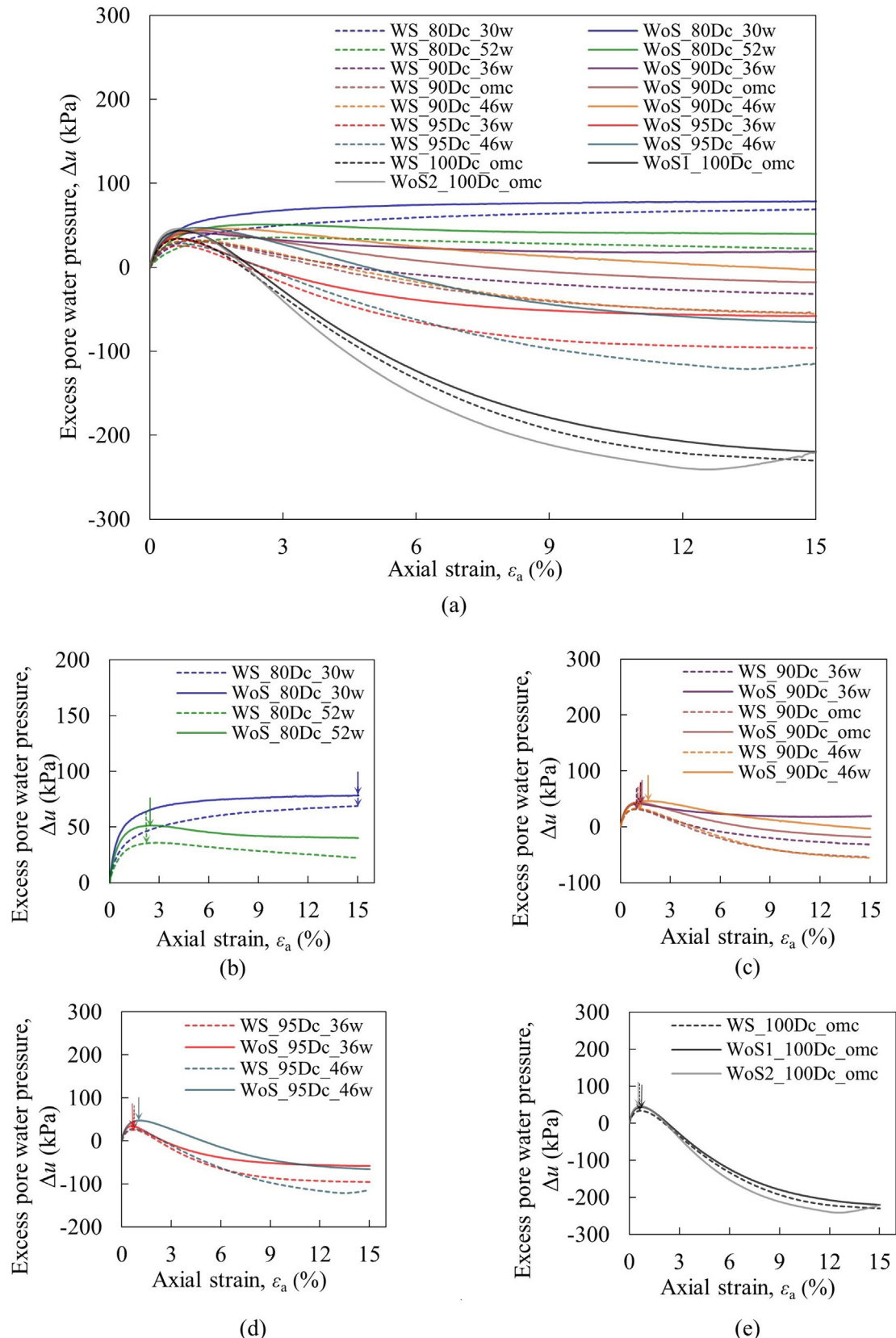


Fig. 22. Relationship between excess pore water pressure and axial strain (a) all specimens, (b) $D_c \approx 80\%$ showing respective PTPs, (c) $D_c \approx 90\%$ showing respective PTPs, (d) $D_c \approx 95\%$ showing respective PTPs, and (e) $D_c \approx 100\%$ showing respective PTPs.

Table 4

Excess pore water pressure and corresponding strain of each specimen.

Specimen identity	Excess PWP at PTP, Δu_{PTP} (kPa)	Axial strain at PTP, $\varepsilon_{a,PTP}$ (%)	Excess PWP at 15 % strain, $\Delta u_{15\%}$ (kPa)	Change in excess PWP, (kPa)	Normalized change in excess PWP
WS_80Dc_30w	(69.4)*	(15)*	69.4	(0)*	(0)*
WoS_80Dc_30w	(78.3)*	(15)*	78.3	(0)*	(0)*
WS_80Dc_52w	35.9	2.50	22.5	13.4	0.168
WoS_80Dc_52w	51.3	2.75	40.1	11.2	0.140
WS_90Dc_36w	32.4	0.94	-31.7	64.1	0.801
WoS_90Dc_36w	41.3	1.04	19.0	22.3	0.279
WS_90Dc_omc	31.4	0.95	-51.4	82.8	1.035
WoS_90Dc_omc	43.8	1.11	-18.1	61.9	0.774
WS_90Dc_46w	32.8	1.03	-55.3	88.1	1.101
WoS_90Dc_46w	46.4	1.43	-3.0	49.4	0.618
WS_95Dc_36w	25.5	0.68	-95.9	121.4	1.517
WoS_95Dc_36w	34.5	0.62	-58.0	92.5	1.156
WS_95Dc_46w	28.2	0.72	-115.1	143.3	1.791
WoS_95Dc_46w	47.3	1.06	-65.2	112.5	1.406
WS_100Dc_omc	34.0	0.67	-230.0	264.0	3.300
WoS1_100Dc_omc	43.7	0.73	-219.9	263.6	3.295
WoS2_100Dc_omc	45.9	0.66	-219.7	265.6	3.319

* The excess pore water pressure at an axial strain of 15% is regarded as the PTP since it did not appear until the end of the experiment due to contractive behaviour.

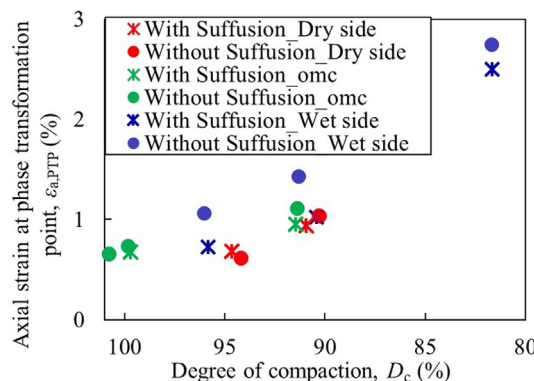


Fig. 23. Relationship between axial strain at phase transformation point and degree of compaction.

strength in suffusion-induced densely compacted pumice sand.

With the migration of fines during suffusion, the particle size ratio (Wiacek and Stasiak, 2018) of the soil decreases due to the comparatively large size and high angularity of the coarse sand particles (Fig. 4), which causes the subsequent increase in the void ratio of the compacted soil (Yilmaz et al., 2023). In addition, the higher value of k for the specimens with suffusion and a lower fines content, in comparison to the value of k for the specimens without suffusion and no change in the fines content (Watabe and Nishimura, 2020), also signifies an increase in pore volume [Fig. 25(b)] due to suffusion. Tsomokos and Georgiannou (2010) stated that grain shape and angularity have a positive effect on the undrained shear behaviour of sand by

increasing the undrained shear strength and exhibiting stable behaviour. Therefore, the strength enhancement of suffusion-induced densely compacted Satozuka pumice sand can be attributed to the alteration of the soil microstructure in the form of the omission of less angular fines, a change in pore volume, and the rearrangement of the highly angular grains brought about by the combined action of hydraulic force and effective stress. This resulted in a decrease in the ratio of rolling to sliding between particles, and a simultaneous improvement in the interlocking of the angular coarse grained particles, thus ensuring a more efficient stress transfer through the soil skeleton made up of coarse grains and greater shear resistance (Mair et al., 2002), as shown in Fig. 26. This change in the soil microstructure correspondingly caused a change in the shearing resistance angle at q_{max} (ϕ_{qmax}), with the maximum shear resistance angle (ϕ_{max}) finally influencing the stress-strain response and stress-dilatancy relation (Yilmaz et al., 2023) which concur with the observations made in this study.

6. Conclusions

Using a modified triaxial setup with the feature of generating suffusion, a series of consolidated undrained triaxial shear tests (\overline{CU} tests) were performed on well-graded densely compacted Satozuka pumice sand containing a high fraction of non-plastic fines. The suffusion characteristics of Satozuka pumice sand and its influence on the mechanical behaviour have led to the following conclusions:

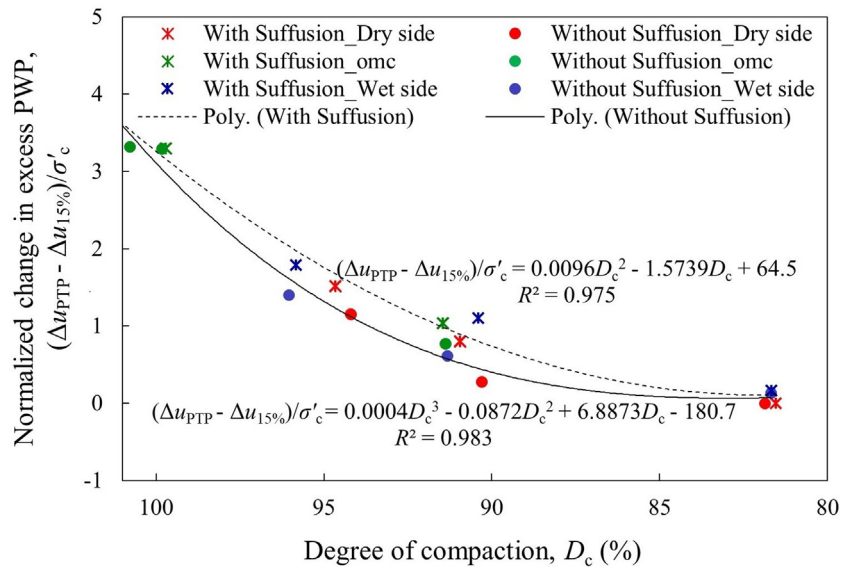


Fig. 24. Relationship between normalized change in excess pore water pressure and degree of compaction.

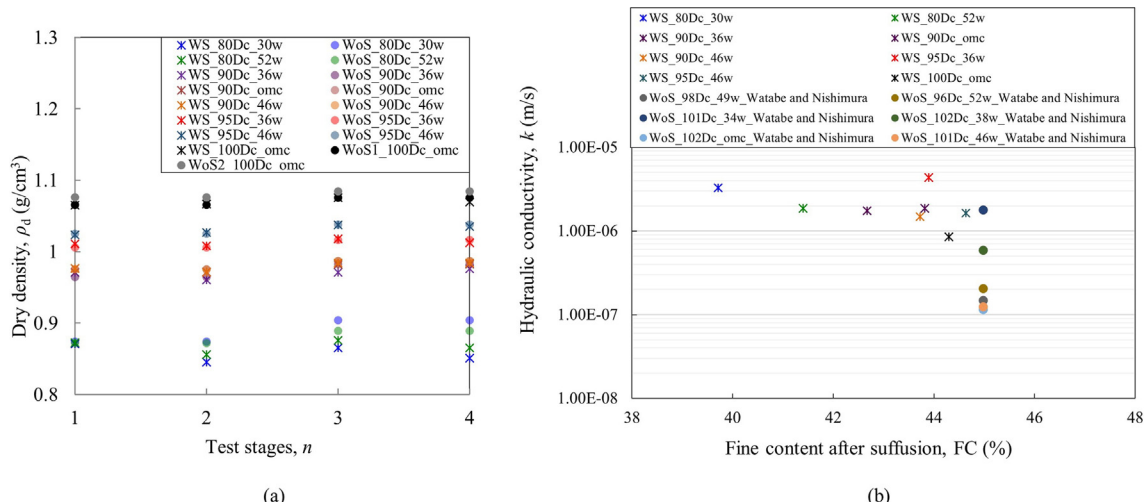


Fig. 25. (a) Variation in dry density of specimens at different stages of experiment, and (b) relationship between hydraulic conductivity and fines content at different degrees of compaction.

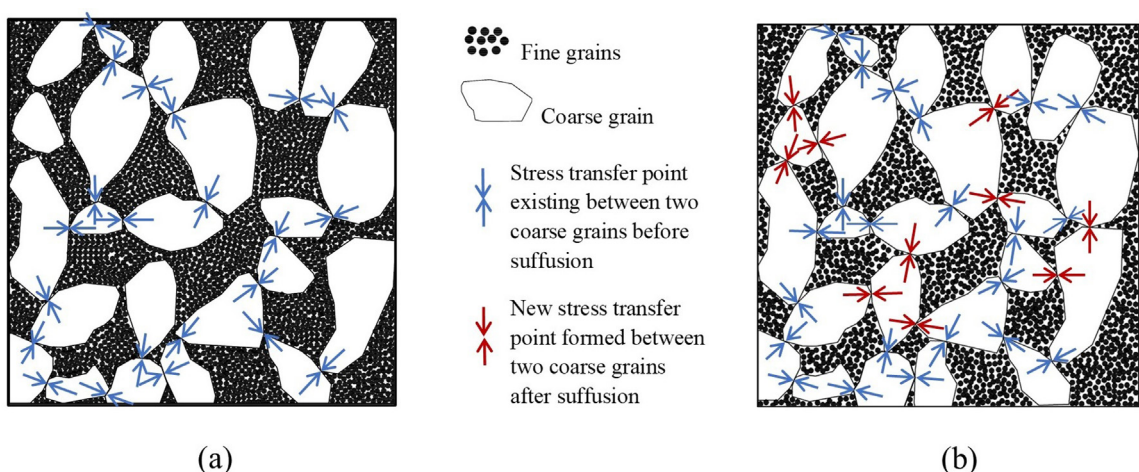


Fig. 26. Changes in soil microstructure and stress transfer mechanism (a) before suffusion, and (b) after suffusion.

- The extent of suffusion increases with a decrease in the degree of compaction D_c during the specimen preparation due to changes in the constriction size and inter-particle grain to grain contact. Furthermore, for equally compact specimens, the degree of saturation S_r (or moisture content) during the specimen preparation adversely affects the extent of suffusion due to the formation of an inter-pore network called macro-porosity in specimens with low saturation.
- Suffusion increases the hydraulic conductivity k of pumice sand by enlarging the flow path (pore diameter of the bottleneck) due to the removal of fines.
- The increase in residual shear strength under undrained shearing for specimens with suffusion indicates that there is no significant negative impact brought about by suffusion on the deterioration of densely compacted earth fill constructed with pumice sand having a high fraction (approximately 45 %) of non-plastic fines. This tendency is consistent for a variety of D_c from 80 % to 100 %. It is noteworthy that the initial D_c has a significant impact on the absolute value of the maximum deviator stress as the increase in density is accompanied by an exponential increase in normalized maximum deviator stress. The normalized maximum deviator stress at the very high density of $D_c > 95\%$ becomes highly sensitive to a minute variation in density as a consequence of this exponential increase and high strength. Densely packed specimens with $D_c > 90\%$ show negligible brittleness irrespective of the suffusion condition. Thus, suffusion exhibits no pronounced influence on the brittleness index.
- The slope of the ESP at q_{max} , M_{qmax} , and the shear resistance angle at q_{max} , ϕ_{qmax} , exhibit higher values for specimens with suffusion up to $D_c \leq 90\%$ and a marginal reduction or no change at all to these values for specimens with suffusion at $D_c \geq 95\%$. In addition, the slopes of the ESP and the shear resistance angles show increments with a rise in density for the specimens both with and without suffusion.
- The dilation tendency of densely compacted pumice sand is enhanced by suffusion. During undrained shear, the specimens undergoing suffusion reach the phase transformation point at a lower axial strain ($\epsilon_{a,PTP}$) than the specimens without suffusion, indicating that the change in volume from contraction to dilation (or phase transformation) occurs earlier in specimens with suffusion.

Declaration of Competing Interest

The authors declare that they have no known competing financial interests or personal relationships that could have appeared to influence the work reported in this paper.

Acknowledgements

The authors are grateful to Prof. S. Nishimura of Hokkaido University for the development and modification of the Visual Basic control program of the triaxial apparatus and guidance with the stereophotogrammetry data analysis. In addition, the authors acknowledge and offer their thanks to Prof. T. Mukunoki of Kumamoto University for conducting the X-ray CT scan of the soil specimens. This research was supported by JST SPRING, Grant Number JPMJSP2119 (Hokkaido University DX Doctoral Fellowship), JSPS KAKENHI Grant Number 21H01421, and City of Sapporo administration, Japan. The authors appreciate the sharing of the initial site investigation data by Oyo Corporation, Japan.

Appendix I.

<i>List of symbols and notations</i>			
A	Area of the specimen	q_R	Residual shear strength
CSL	Critical state line	S_r	Degree of saturation
C_c	Coefficient of curvature	t	Flow duration
C_u	Coefficient of uniformity	u, v	2-dimensional coordinates in image space
D	Soil particle diameter	V_e	Volume of effluent
D_c	Degree of compaction attained after specimen preparation	w	Moisture content
$D_{c,t}$	Target degree of compaction	WoS	Without suffusion
D_r	Relative density	WS	With suffusion
FC	Fines content	X_w, Y_w, Z_w	3-dimensional coordinates of target point in real physical space
ESP	Effective stress path	Δm_d	Change in dry mass of specimen
I_B	Brittleness index	ΔV	Change in volume of specimen
i	Target point in stereophotogrammetry	Δu	Excess pore water pressure
i	Hydraulic gradient	$\Delta u_{15\%}$	Excess PWP at 15 % strain
k	Coefficient of hydraulic conductivity	Δu_{PTP}	Excess PWP at PTP
M_{max}	Maximum slope of ESP	ϵ_a	Axial strain

$M_{q\max}$	Slope of ESP at q_{\max}	$\varepsilon_{a,PTP}$	Axial strain at PTP
m_d	Dry mass of specimen	ε_r	Radial strain
n	Number of stages	ε_v	Volumetric strain
OMC	Optimum moisture content	ρ_d	Dry density
p'	Effective mean stress	$\rho_{d\max}$	Maximum dry density
PWP	Pore water pressure	ρ_{\max}	Maximum density
PTP	Phase transformation point	ρ_{\min}	Minimum density
Q	Flow rate	σ'_c	Effective consolidation stress
q	Deviator stress	ϕ_{\max}	Maximum shear resistance angle
q_{\max}	Maximum deviator stress	$\phi_{q\max}$	Shear resistance angle at q_{\max}

5-mm intervals (and a reference target line with red dots) on the rubber membrane.

The two sets of cameras (front camera set and rear camera set) at an approximate angle of 45° were placed on two sides of the triaxial cell at a distance of 200–250 mm [Fig. 28(a)]. The ray-tracing technique was adopted to correct the ray refraction due to interfaces (air and cell wall, cell wall, and water). The cameras were calibrated using a calibration sheet with targets at the known intervals. The images were recorded at 1-minute intervals [e.g., Fig. 28 (b)]. The cameras can identify a common target point with u, v coordinates in image space (stereo-matching) using a pinhole camera model. The target points determined from the obtained images were converted into binary pixels, and the coordinates were computed in $u-v$ space with the aid of digital image correlation (DIC). The strain values on an element with $i = 1-4$ were obtained from the reference state and current state of the target points (1, 2, 3, and 4) using Eqs. (9) and (10) (Nishimura, 2022), as shown in Fig. 27(b), followed by the reconstruction of the 3-dimensional images of the specimens in terms of the elements (Fig. 14) in Python.

Axial strain,

$$\varepsilon_a = -\frac{1}{2} \sum_{i=1}^2 \frac{(Y_{w,2i} - Y_{w,2i-1}) - (Y_{w0,2i} - Y_{w0,2i-1})}{(Y_{w0,2i} - Y_{w0,2i-1})} \quad (9)$$

Radial strain,

$$\varepsilon_r = -\frac{1}{4} \sum_{i=1}^4 \frac{\sqrt{(X_{w,i}^2 + Z_{w,i}^2)} - \sqrt{(X_{w0,i}^2 + Z_{w0,i}^2)}}{\sqrt{(X_{w0,i}^2 + Z_{w0,i}^2)}} \quad (10)$$

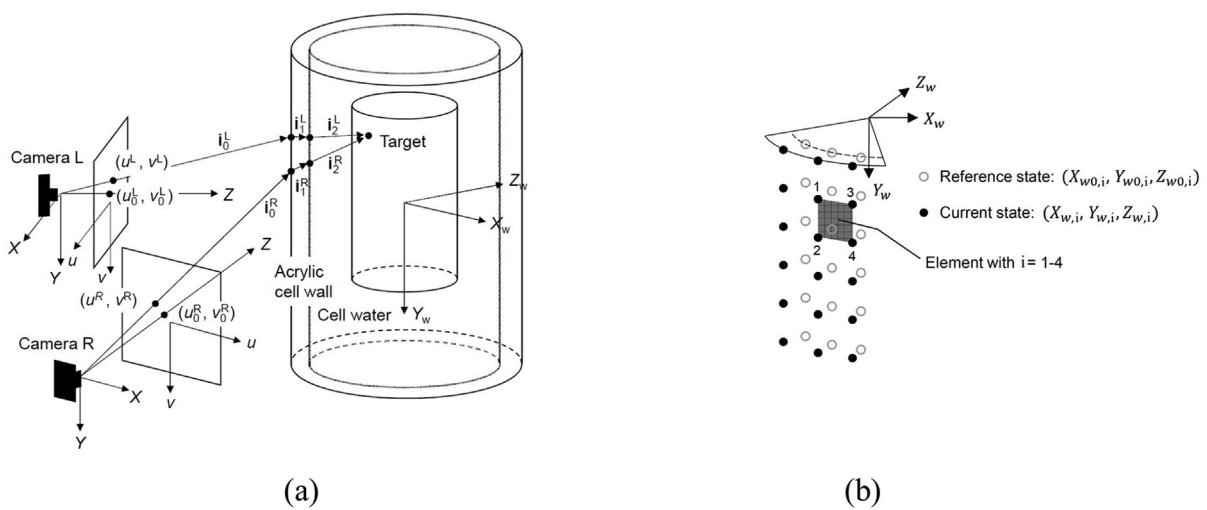


Fig. 27. (a) Graphical representation of stereophotogrammetry in geometry, and (b) reference state and current state of target points (Nishimura, 2022).

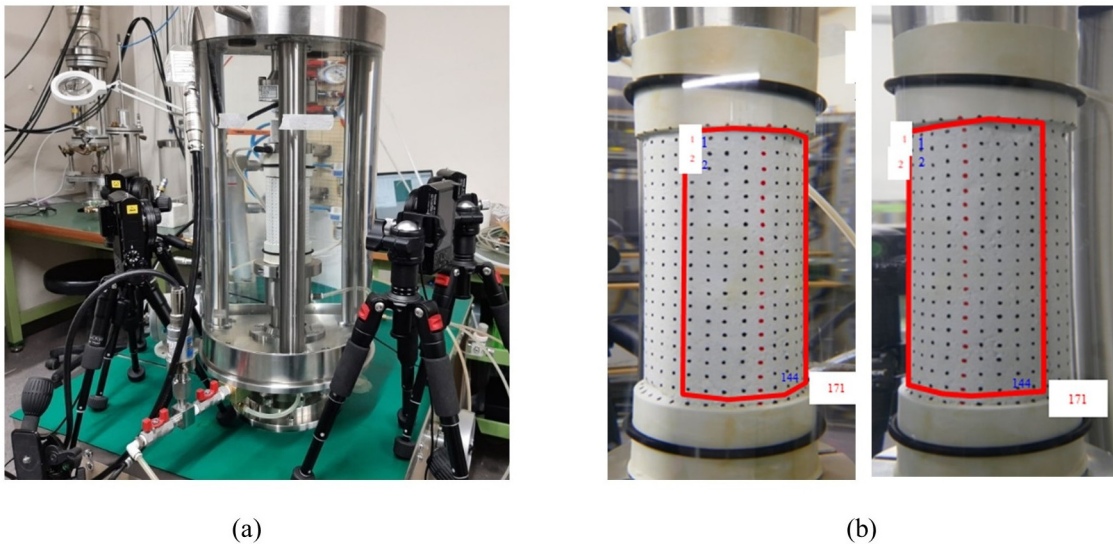


Fig. 28. (a) Camera setup, and (b) stereo images captured by front camera set (camera L and camera R) used in this study.

where $X_{w0,i}$, $Y_{w0,i}$, and $Z_{w0,i}$ are the reference states, and $X_{w,i}$, $Y_{w,i}$, and $Z_{w,i}$ are the current states of any target point i , as shown in Fig. 27(b).

References

- Bedja, M., Umar, M., Kuwano, R., 2022. Influence of density on the post-suffusion behavior of gap-graded sand with fines. *Soils Found.* 62 (3). 101159. <https://doi.org/10.1016/j.sandf.2022.101159>.
- Bishop, A.W., 1967. Progressive failure with special reference to the mechanism causing it. *Proceeding of the Geotechnical Conference, Norwegian Geotechnical Institute, Oslo 2*, 142–150.
- Bolton, M.D., 1986. Strength and dilatancy of sands. *Geotechnique* 36 (1), 65–78.
- Chang, D.S., Zhang, L.M., 2011. A stress controlled erosion apparatus for studying internal erosion in soils. *Geotech. Test. J.* 34 (6), 579–589.
- Chitravel, S., Otsubo, M., Kuwano, R., 2021. Experimental study on stiffness degradation and monotonic response of reconstituted volcanic ash induced by internal erosion. *Soils Found.* 61 (5), 1431–1452. <https://doi.org/10.1016/j.sandf.2021.08.003>.
- Cubrinovski, M., Rees, S., Bowman, E., 2010. Effects of non-plastic fines on liquefaction resistance of sandy soils. *Earthquake Engineering in Europe. Geotechnical, Geological, and Earthquake Engineering*, Garevski M. and Ansal A. (eds) Springer, Dordrecht, 17, 125–144. https://doi.org/10.1007/978-90-481-9544-2_6.
- Daouadji, A., Jrad, M., Robin, G., Brara, A., Daya, E.M., 2016. Phase Transformation States of Loose and Dense Granular Materials under Proportional Strain Loading. *J. Eng. Mech.* 143 (1). [https://doi.org/10.1061/\(ASCE\)EM.1943-7889.0001056](https://doi.org/10.1061/(ASCE)EM.1943-7889.0001056).
- Elgamal, A., Dobry, R., Parra, E., Yang, Z., 1998. Soil dilation and shear deformations during liquefaction. *International Conference on Case Histories in Geotechnical Engineering*. 10. <https://scholarsmine.mst.edu/iccge/4icchge/4icchge-session03/10>.
- Japanese Industrial Standards. 2009. JIS A 1210: 2009. Test method for soil compaction using a rammer (in Japanese).
- Japanese Industrial Standards. 2009. JIS A 1224: 2009. Test method for minimum and maximum densities of sands (in Japanese).
- Ke, L., Takahashi, A., 2014. Triaxial erosion test for evaluation of mechanical consequences of internal erosion. *Geotech. Test. J.* 37 (2), 1–18.
- Kuwano, R., Spitia, L.F.S., Bedija, M., Otsubo, M., 2020. Change in mechanical behaviour of gap-graded soil subjected to internal erosion observed in triaxial compression and torsional shear. *Geomech. Energy Environ.* 27 (2021). 100197. <https://doi.org/10.1016/j.gete.2020.100197>.
- Mair, K., Frye, K.M., Maronez, C., 2002. Influence of grain characteristics on the friction of granular shear zones. *Journal of Geophysical Research* 107 (10), 41–49. <https://agupubs.onlinelibrary.wiley.com/doi/full/10.1029/2001JB000516>.
- Marot, D., Bendahmane, F., Nguyen, H.H., 2012. Influence of angularity of coarse fraction grains on internal erosion process. *International Conference on Scour and Erosion (ICSE-6)*, <https://hal.science/hal-01716703>.
- Miedema, R., Oort, F.V., 1990. Significance of Soil Microfabric for Soil Physical Characteristics and Behaviour of Late Weichselian and Holocene Rhine Deposits in the Netherlands. *Dev. Soil Sci.* 19, 97–105. [https://doi.org/10.1016/S0166-2481\(08\)70320-9](https://doi.org/10.1016/S0166-2481(08)70320-9).
- Nishimura, S., 2022. Characterisation of soil deformation over wide strain ranges in triaxial test with high-precision stereophotogrammetry. *Geotechnique*, (Published online on 21 April 2022) 0 0:0, 1–16. <https://doi.org/10.1680/jgeot.21.00067>.
- Picarelli, L., Olivares, L., Lampitello, S., Darban, R., Damiano, E., 2020. The undrained behaviour of an air-fall volcanic ash. *Geosciences* 10 (2), 60. <https://doi.org/10.3390/geosciences10020060>.
- Romero, E., Gens, A., Lioret, A., 1999. Water permeability, water retention and microstructure of unsaturated compacted Boom clay. *Eng. Geol.* 54 (1–2), 117–127. [https://doi.org/10.1016/S0013-7952\(99\)00067-8](https://doi.org/10.1016/S0013-7952(99)00067-8).
- Sarmah, R., Kubota, S., Watabe, Y., 2021. Influence of suffusion on shear strength and dilatancy characteristics of pumice sand. *Proceedings of the 10th International Conference on Scour and Erosion (ICSE-10)*, Rice, J., Liu, X., McIlroy, M., Sasanakul, I., and Xiao, M. (eds), Arlington, Virginia, USA. 18–21 October, 2021. 1034–1043. https://www.issmge.org/uploads/publications/108/109/Influence_of_Suffusion_on_Shear_Strength_and_Dilatancy_Characteristics_of_Pumice_Sand.pdf.
- Sato, M., Kuwano, R., 2018. Laboratory testing for evaluation of the influence of a small degree of internal erosion on deformation and stiffness. *Soils Found.* 58, 547–562.
- Skempton, A.W., 1954. The pore-pressure coefficients A and B. *Géotechnique* 4 (4), 143–147. <https://doi.org/10.1680/geot.1954.4.4.143>.
- Sladen, J.A., D'Hollander, R.D., Krahn, J., 1985. The liquefaction of sands, a collapse surface approach. *Can. Geotech. J.* 22, 564–578. <https://doi.org/10.1139/t85-076>.

- Tamura, T., Sakai, T., 1992. Measurement of the degree of compaction by the impedance method. *J. Terramech.* 29 (1), 125–135. [https://doi.org/10.1016/0022-4898\(92\)90020-K](https://doi.org/10.1016/0022-4898(92)90020-K).
- Tang, C.S., Lin, L., Cheng, Q., Zhu, C., Wang, D.W., Lin, Z.Y., 2020. Quantification and characterizing of soil microstructure features by image processing technique. *Comput. Geotech.* 128 (2020). 103817. <https://doi.org/10.1016/j.comgeo.2020.103817>.
- Tatsuoka, F., Fujishiro, K., Tateyama, K., Kawabe, S., Kikuchi, Y., 2016. Properties of compacted soil as a function of dry density and the degree of saturation. Japanese Geotechnical Society Special Publication, Proceedings of the 15th Asian Regional Conference on Soil Mechanics and Geotechnical Engineering 2 (4), 247–252 <https://doi.org/10.3208/jgssp.JPN-099>.
- Tsomokos, A., Georgiannou, V.N., 2010. Effect of grain shape and angularity on the undrained response of fine sands. *Can. Geotech. J.* 47 (5), 539–551. <https://doi.org/10.1139/T09-121>.
- Watabe, Y., Soesilo, E.G., Sassa, S., 2021. Influence of compaction conditions on erodibility of clayey sand. Proceedings of the 10th International Conference on Scour and Erosion (ICSE-10), Rice, J., Liu, X., McIlroy, M., Sasanakul, I., and Xiao, M. (Eds.), Arlington, Virginia, USA. 18–21 October, 2021. 991–1000.
- Watabe, Y., Nishimura, S., 2020. Ground movements and damages in Satozuka District, Sapporo, due to 2018 Hokkaido Eastern Iburi Earthquake. *Soils Found.* 60, 1331–1356. <https://doi.org/10.1016/j.sandf.2020.04.007>.
- Wiącek, J., Stasiak, M., 2018. Effect of the particle size ratio on the structural properties of granular mixtures with discrete particle size distribution. *Granul. Matter* 20 (31). <https://doi.org/10.1007/s10035-018-0800-7>.
- Xiao, Y., Liu, H., Chen, Y., Chu, J., 2014. Strength and Dilatancy of Silty Sand. *J. Geotech. Geoenvir. Eng.* 140 (7). [https://doi.org/10.1061/\(ASCE\)GT.1943-5606.0001136](https://doi.org/10.1061/(ASCE)GT.1943-5606.0001136).
- Xiao, M., Shwiyhat, N., 2012. Experimental investigation of the effects of suffusion on physical and geomechanic characteristics of sandy soils. *Geotech. Test. J.* 35 (6), 1–11. <https://doi.org/10.1520/GTJ104594>.
- Yamamuro, J.A., Lade, P.V., 1997. Static liquefaction of very loose sands. *Can. Geotech. J.* 34, 905–917.
- Yilmaz, Y., Deng, Y., Chang, C.S., Gokce, A., 2023. Strength–dilatancy and critical state behaviours of binary mixtures of graded sands influenced by particle size ratio and fines content. *Géotechnique* 73 (3), 202–217. <https://doi.org/10.1680/jgeot.20.P.320>.
- Yoshimine, M., Robertson, P., 1999. Undrained shear strength of clean sands to trigger flow liquefaction. *Can. Geotech. J.* 36, 891–906.
- Zhong, C., Le, V.T., Bendahmane, F., Marot, D., Yin, Z.Y., 2018. Investigation of spatial scale effects on suffusion susceptibility. *J. Geotech. Geoenvir. Eng.* 144 (9), 04018067-1–10. [https://doi.org/10.1061/\(ASCE\)GT.1943-5606.0001935](https://doi.org/10.1061/(ASCE)GT.1943-5606.0001935).